DeMeo Taxonomy: Categorization of Asteroids in the Near-Infrared

By

Francesca E. DeMeo

B.S., Earth, Atmospheric and Planetary Sciences (2006)
B.S., Physics (2006)

Massachusetts Institute of Technology

Submitted to the Department of Earth, Atmospheric and Planetary Sciences
in Partial Fulfillment of the Requirements for the Degree of
Master of Science in Earth, Atmospheric, and Planetary Sciences

at the

Massachusetts Institute of Technology

June 2007

Author _____
Department of Earth, Atmospheric and Planetary Sciences
June 2007

Certified by _____
Professor Richard P. Binzel
Thesis Supervisor

Accepted by _____
Maria T. Zuber
E.A. Griswold Professor of Geophysics
Head, Department of Earth, Atmospheric & Planetary Sciences

Table of Contents

DeMeo Taxonomy: Categorization of Asteroids in the Near-Infrared

By
Francesca E. DeMeo

Submitted to the
Department of Earth, Atmospheric and Planetary Sciences

June 2007

In Partial Fulfillment of the Requirements for the Degree of
Master of Science in Earth, Atmospheric, and Planetary Sciences

Abstract

This work presents the DeMeo taxonomy, an asteroid taxonomy with 24 classes based on Principal Component Analysis of spectral data over the visible and near-infrared wavelengths, specifically the 0.45 to 2.45 micron range. Principal Component Analysis was used by both Tholen (1984) and Bus (1999) to create taxonomies on visible data. There is no pre-existing taxonomic system for the entire suite of asteroid characteristics because only in the current decade has spectral data collection become available in the near-infrared for asteroids down to relatively faint (V=17) limiting magnitudes. (Rayner et al. 2003) With a larger data range, which includes important absorption features at one and two microns suggesting the presence of minerals, there is a need for an extended system to encompass this range of information. In this work we explain the process of creating the taxonomy, the method for finding an object's taxonomic class under this system, and present spectral types for the 365 objects that were used to create the system.

Thesis Supervisor: Richard P. Binzel
Title: Professor of Planetary Science

Acknowledgements

I am grateful for the help and advice from many colleagues and students. I thank Bobby Bus for all his guidance and the expertise he provided having created a previous taxonomic system. Thanks to Pierre Vernazza for all the mineralogical background and input he contributed which helped me understand the distinctions between spectra. Thanks to Cristina Thomas for always being available to help me with any problems or questions and for always taking the tough night shift during observing runs. I thank Shaye Storm for being a great UROP student and for helping me reduce and organize the data for this work. I would also like to thank many others who have taught me much and helped me along the way. Thanks Andy Rivkin, Mike Person, Steve Slivan, Jim Elliot, Jack Wisdom, Elisabeth Adams, Mark Avnet, and Susan Kern. I thank my family for everything.

I also owe huge thanks to my advisor Professor Rick Binzel who has guided me through not just my Masters thesis, but also my senior thesis. Thank you Rick for all the opportunities you have provided for me, the chance to visit the IRTF on Mauna Kea and Magellan in Chile, to travel to and present at conferences, to research in France and meet colleagues. Thank you for always taking the time to help and answer questions, for going out of your way to make sure you're available to help, for always being patient, and for always being accommodating for the projects I undertake and plans I make outside of my research. And by the way, that is a sweet Earth.

1. Introduction

Classification is important to all branches of sciences. As soon as a large amount of data are available, it is useful to group it into categories with similar characteristics for organization, comparison, and better comprehension.

The first asteroid taxonomy was created by Chapman et al. (1975). The taxonomy has grown and evolved over time to account for more and better data. Asteroid scientists started by characterizing asteroids with a few colors, and then many colors as technology improved. Some taxonomies incorporated albedo, and eventually they used spectra. Taxonomies were created by Tholen (1984) and most recently by Bus (1999). All current asteroid taxonomies are based on the visible wavelength range approximately 0.4 to 0.9 microns because data were most available over those wavelengths. Recently, with the creation of the SpeX instrument on the IRTF a growing library has been created of near-infrared spectral data. Gaffey et al. (1993) created an S-complex taxonomy based on near-infrared data, but there is no pre-existing taxonomic system for the entire suite of asteroid characteristics. From Figures 1 and 2 we can see examples of the need for a new taxonomy because of the divergence in the near-infrared of a single well-constrained visible class. A classification system that extends to the near-infrared is also important because significant mineral absorption features are present at one and two microns suggesting presence of pyroxene and olivine. Even though the taxonomy presented in this work is not connected to mineralogy it is hoped that future work would allow mineralogic interpretation of taxonomic classes.

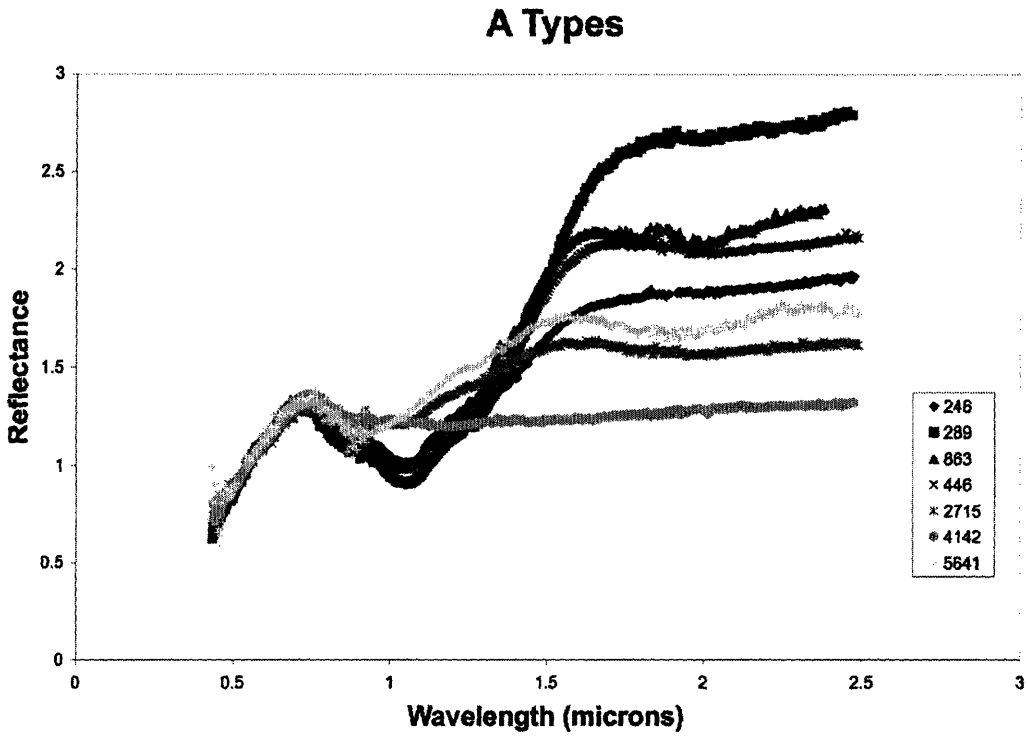

Figure 1: Bus Taxonomy A-Types. All spectra behave similarly in the visible and are designated A-Types in the Bus system, but have very different behaviors in the near-infrared.

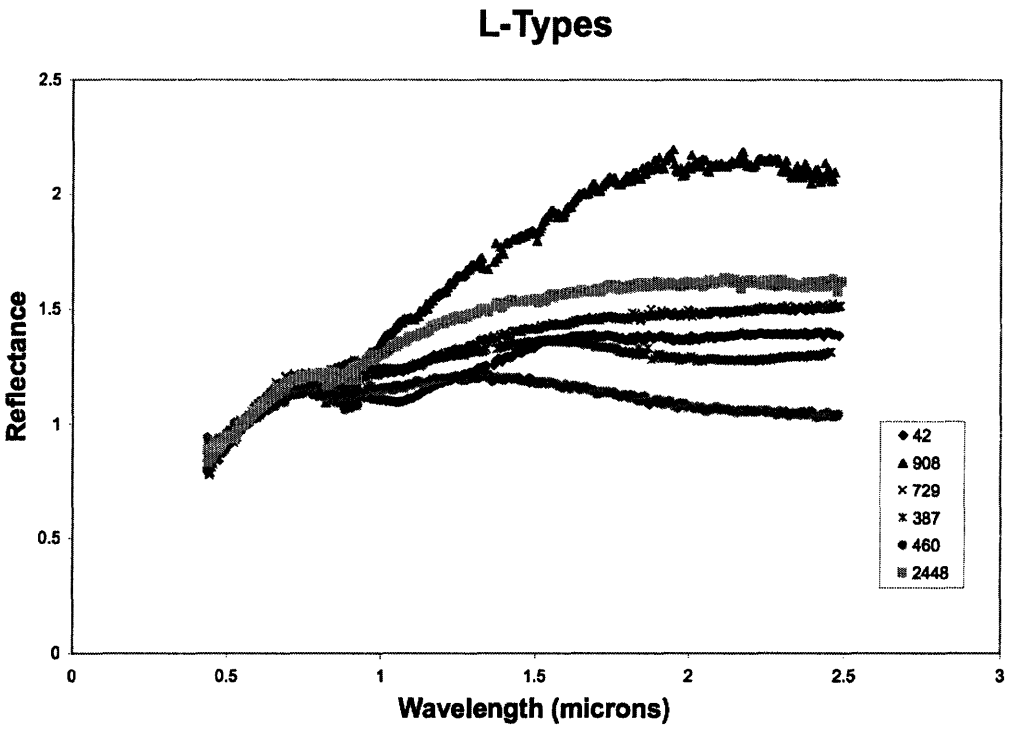

Figure 2: Bus Taxonomy L-Types. This plot shows L-types under the Bus classification system. Notice how well they match in the visible range, but diverge in the near-infrared. Some have stronger 1 micron absorptions, some have high slopes or even negative slopes after one micron.

This work presents the DeMeo taxonomy, an asteroid taxonomy based on Principal Component Analysis of spectral data over the visible and near-infrared wavelengths, specifically the 0.45 to 2.45 micron range. The aim of this new taxonomy is to have classification parameters for the entire wavelength range, but not to create an entirely new system. Principal Component Analysis (PCA) is a technique for reducing the dimensionality of a dataset to contain most of the information in a few principal components. It is a set of linear transformations changing the coordinate system according to the greatest variance. The greatest variance is along the dimension

described by Principal Component 1 and the second greatest variance is Principal Component 2. PCA is used widely in other applications such as data compression, but was not applied to the field of asteroid taxonomy until Tholen (1984).

When creating this taxonomy there were seven possible outcomes for changes to each taxonomic class under the Bus system. Two classes could be indistinguishable over the entire wavelength range and merge into one class. One class could be degenerate and branch off into two (or more) separate classes. A class may need to be created if spectra exist that do not fit within the past framework. We found that one new class needed to be created, the Sv class, comprised of two objects that represented an intermediate class between S and V. The name of a class may need to be changed if the current notation seems misleading. Some classes may need to be redefined. For example the names Sr and Sa were conserved but the objects in those classes were largely redefined. There is the possibility that one class may correlate directly as near-infrared data are included and no change in that class occurs. Finally, it is possible that a class may remain the same, but a notation is added. In this taxonomy a "w" notation was used to indicate high slope and is explained in Section 4. Figure 3 is a diagram of the possible outcomes of extending the classes. See Appendix A for the progression from the Bus to DeMeo taxonomy.

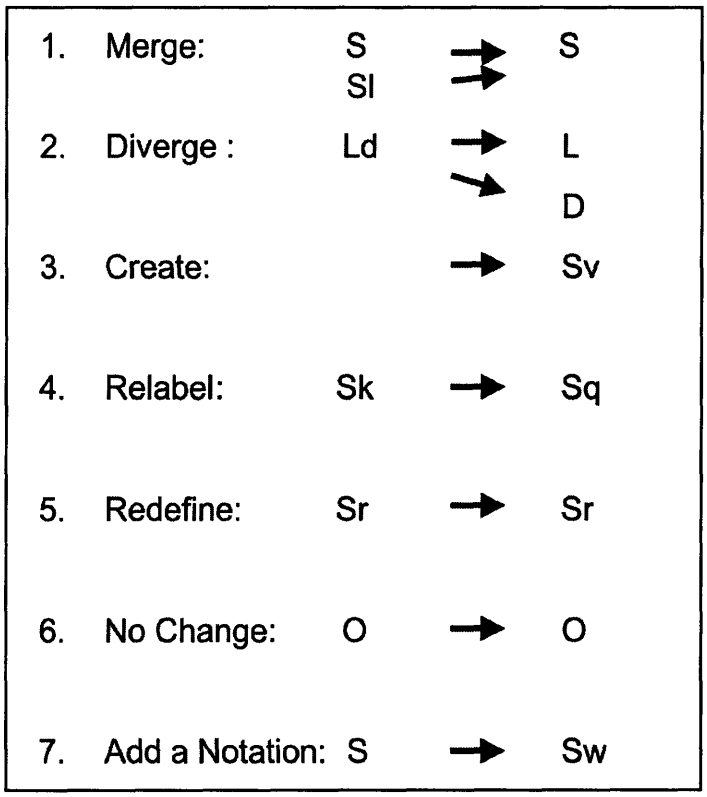

Figure 3: Possible outcomes of extending taxonomic classification to the near-infrared. 1. Two classes from the Bus system could merge to one class. 2. One class could diverge into two distinct classes. 3. A class that did not previously exist may be created. 4. A previously existing class may be relabeled with a different name. 5. A class may keep its label but its definition may change. 6. One class could correlate directly from the Bus to DeMeo taxonomies. 7. An additional notation to may be added within a class.

2. Observations and Data Reduction

Near-infrared spectral measurements from 0.8 to 2.5 microns were obtained using the SpeX instrument on the 3 meter NASA Infrared Telescope Facility (IRTF) located on Mauna Kea, Hawaii. As described in DeMeo and Binzel (2007), when possible, objects and standard stars were observed near the meridian to minimize their differences in airmass. Frames were taken so that the object was alternated between two different positions (usually noted as the 'A' and 'B' positions) on a 0.8 x 15 arcsecond slit aligned north-south. Solar-type standard stars were observed to divide the solar spectrum from

the asteroid spectra, with the result being reflectance spectra. Our primary solar analog standard stars were 16 Cyg B and Hyades 64. Additional solar analog stars were utilized around the sky, having comparable spectral characteristics. Two to three sets of eight images per set were taken for each object, with individual image exposures typically being 120 seconds. The total integration time for each of these objects therefore ranged from 30 to 120 minutes.

Reduction was performed using a combination of routines within the Image Reduction and Analysis Facility (IRAF), provided by the National Optical Astronomy Observatories (NOAO) (Tody 1993), and Interactive Data Language (IDL). We use a software tool called "autospex" to streamline reduction procedures outlined by S. J. Bus (personal communication). Autospex writes macros containing a set of IRAF (or IDL) command files that are then executed by the image processing package. Autospex procedures operate on a single night at a time, with the opportunity for the user to inspect and verify the results at each stage. Briefly, autospex writes macros that: trim the images down to their useful area, create a 'bad pixel map' from flat field images, flat field correct all images, perform the sky subtraction between AB image pairs, register the spectra in both the wavelength and spatial dimensions, co-add the spectra for individual objects, extract the 2-D spectra from co-added images, and then apply the final wavelength calibration. Using IDL, an absorption coefficient is determined for each object and star pair that best minimizes atmospheric water absorption effects for that pair. This coefficient correction is most important near 1.4 and 2.0 microns, locations of major absorption bands due to telluric H_2O. Because we operate in survey mode with our observing time heavily weighted toward new objects rather than on standard stars, our

telluric corrections are not perfect. Users of these data therefore must exercise caution in basing significant scientific conclusions on any unusual spectral features at these telluric wavelengths, which may be the result of imperfect correction. The last IDL step averages all the object and standard pairs to create the final reduced spectrum for each object.

All visible wavelength spectra (usually 0.4 to 0.9 microns) were taken from the Small Main Belt Asteroid Spectroscopic Survey (SMASS II) data set (Bus & Binzel 2002). Our sample was comprised of 365 objects with both visible and near-IR data. For a table of observations see Appendix B.

3. Background on Classification

3.1 Thoughts on Classification

Classification systems tend to emerge as soon as there are enough data to form groups. It is a tool used to organize information making it easier to compare, find holes or missing information, and makes it easier to communicate about data features.

Data on asteroids come from three sources: spacecraft missions, meteorites, and telescope observations. Spacecraft missions provide the most detailed information about asteroids, however, they only reach a limited number of targets. Meteorites provide a great opportunity for detailed study in a laboratory, but their links to specific asteroids and even general asteroid classes are nonexistent or weak. The only known connection between a meteorite and its parent asteroid are the HED meteorites to Vesta (Consolmagno & Drake 1977, Binzel & Xu 1993) Telescope observations provide data including brightness, albedo, and spectral reflectance on a large number of asteroids making it the best basis for classification of many objects.

The purpose of this classification system is to characterize the features present in the spectrum. These features may represent mineralogy, grain size, weathering, or other properties of or effects on an asteroid, however the taxonomy is not meant to suggest or confirm anything more than the features visible in the spectrum.

3.2 Previous Classification Systems

Asteroid taxonomy has evolved significantly over the past few decades, as more and higher quality data have become available. Starting in the 1950's UBV photometry observations enabled the separation of asteroids into two groups noted by Wood and Kuiper (1963) and Chapman et al. (1971). Using spectrophotometry and albedo measurements Chapman et al. (1975) created the first letter-based asteroid taxonomy. "C" represented carbonaceous, "S" was for stony, and "U" for unusual objects. Tholen Taxonomy was the most widely used when created with eight classes of spectral types, plus classes for three unusual objects. The Barucci Taxonomy, meant to expand on the Tholen taxonomy was based on G-mode analysis. (Tholen & Barucci 1989, Barucci et al. 1987). The most recent taxonomy was created by Bus using 1189 objects. It is feature-based taxonomy also using PCA (Bus 1999, Bus & Binzel 2002). The Bus system further separated the C, S, and X complexes.

Only in the current decade has spectral data collection become available in the near-infrared for asteroids down to relatively faint (V=17) limiting magnitudes. (Rayner et al. 2003) With a larger data range, which includes important absorption features, there is a need for an extended system to encompass this range of information. We chose not to

invent an entirely new system, but instead strove to stay as consistent as possible with past visible taxonomies and notation.

3.3 Process To New Classification

3.3.1 PCA Preparation

Bus chose three prototype asteroids for each of his taxonomic classes that best exemplify the characteristics of the class. The process of creating a new taxonomy began with the evaluation of the Bus prototypes over the entire wavelength range. Some of these prototypes had to be rearranged and redesignated. Asteroid 150, for example, was a Cb under the Bus system, but looks much more like a C over the entire range. Asteroid 24 was a B and is now a C. 42 was an L and is now a K. 606 was a K and was redesignated to L. 1904 and 5111 were R-types and are now V. Even though there were many changes, most were within subclasses or closely related classes. This exercise was mainly to observe how each class behaved in the near-infrared and which classes were more or less well-defined. Because the new system has many more features present in the near-infrared than the visible it is natural that some objects that looked similar in the visible diverge in the near-infrared.

Next, to become more familiar with the data, we assigned a taxonomic type or complex by visually assessing spectral features and plotting it against prototypes. This was useful because when plotting objects in PCA space we could compare how objects grouped when labeled under the Bus system with what we believed they looked like in the visible and near-infrared range.

We then plotted all near-infrared data in a "splinefit" program which creates a list of data points that follow the features of the spectrum. This step smoothes the spectra, creating a good "best fit" curve to the data. This reduces the risk of noise or missing data points influencing the PCA. We sampled the region 0.45 to 2.45 microns and recorded points at increments of 0.05 resulting in 41 channels.

The "splined" data were then normalized at 0.55 microns and the slope was removed from the data and recorded. With our normalized data we simply took a linear regression line of each set of data. Because this is the most prominent feature of the spectra we can remove it from the data before performing principal component analysis thus making PCA more sensitive to other features, and therefore more effective. We divide all the data points by the average slope. The remaining data are a horizontal spectrum with residuals (including absorption features) above and below the horizontal. We now have data with slope removed having 41 channels normalized at 0.55 microns. Because each spectrum has a value of 1 at 0.55, that channel provides no new information and so was removed from the data set to make PCA more effective. We therefore input 40 channels per object into PCA

To verify that we could remove the slope before running PCA, we ran PCA on the data without the slope removed. The first principal component (PC1) of PCA before removing slope was compared to the slope we remove directly from the splined data. In Figure 4, a plot of PC1 versus slope, it is clear that the two are linearly correlated, thus PC1 corresponds to slope and we are justified in removing it first.

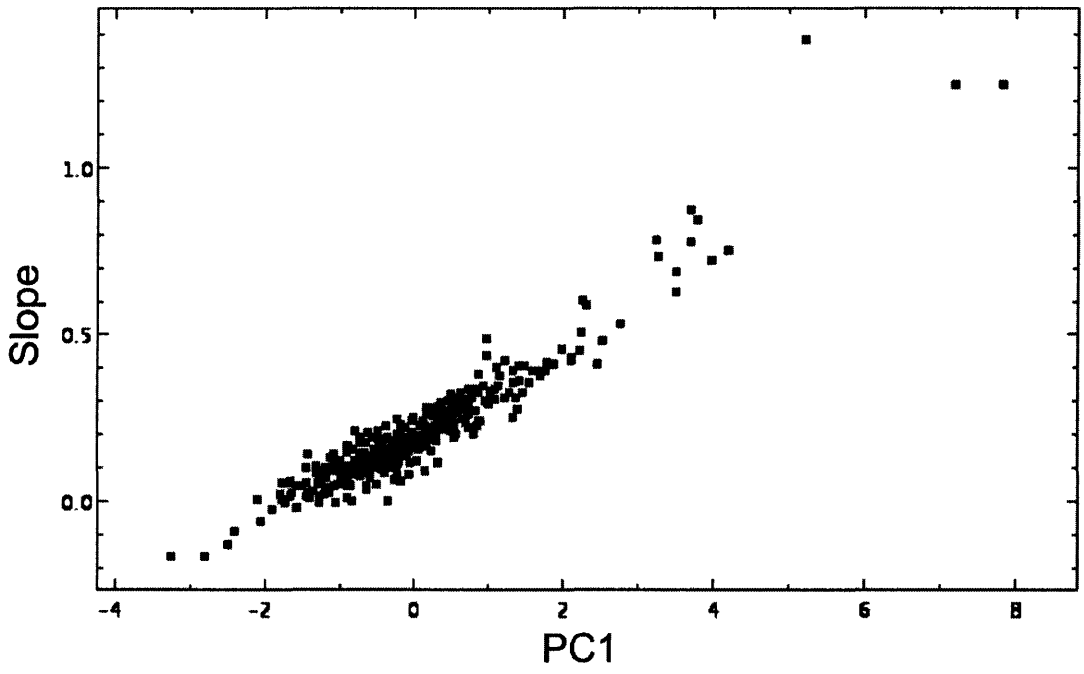

Figure 4: Plot of PC1 versus Slope. PC1 is the first principal component from the data set that did not have the slope removed. It is clear from the plot that PC1 and slope are linearly related and it is thus safe to remove the slope before running PCA to make PCA more sensitive to other features.

Using MATLAB, we performed Principal Component Analysis (PCA) on the splined files with slopes removed. PCA is a method of reducing the dimensionality of a data set. PCA involves coordinate transformations to minimize the variance. The first transformation rotates the data to maximize variance along the first axis, known as Principal Component 1' (PC1'), the second axis is the second Principal Component (PC2'). The first few principal components contain the majority of the information. For a more thorough explanation of PCA and why it is useful for asteroid taxonomy refer to Tholen (1984) and Bus (1999).

3.3.2 What Principal Components Tell

By plotting the principal components against one another we can see how different groups separate. PCA was used to create the Tholen and Bus taxonomies. We chose to use covariance instead of correlation for the PCA. Bus (1999) suggested the use of the covariance matrix of unscaled variances because they may be useful to distinguish spectra. Principal Component Analysis tells information about specific parts of the spectrum. It is difficult to determine what exact feature each principal component refers to because so many features exist over the visible to near-infrared wavelength. However, by looking at the eigenvectors we can determine over which wavelength range each principal component is most sensitive. Figure 5 is a plot of sensitivity of the eigenvectors throughout the range. This figure shows that PC4' and PC5' are more sensitive to features at the ends of the spectrum, while the others are more sensitive to features in the middle. See Appendix C for the eigenvectors. Wavelengths with higher magnitudes dominate that principal component using positive or negative weights to separate in opposite directions within that principal component space.

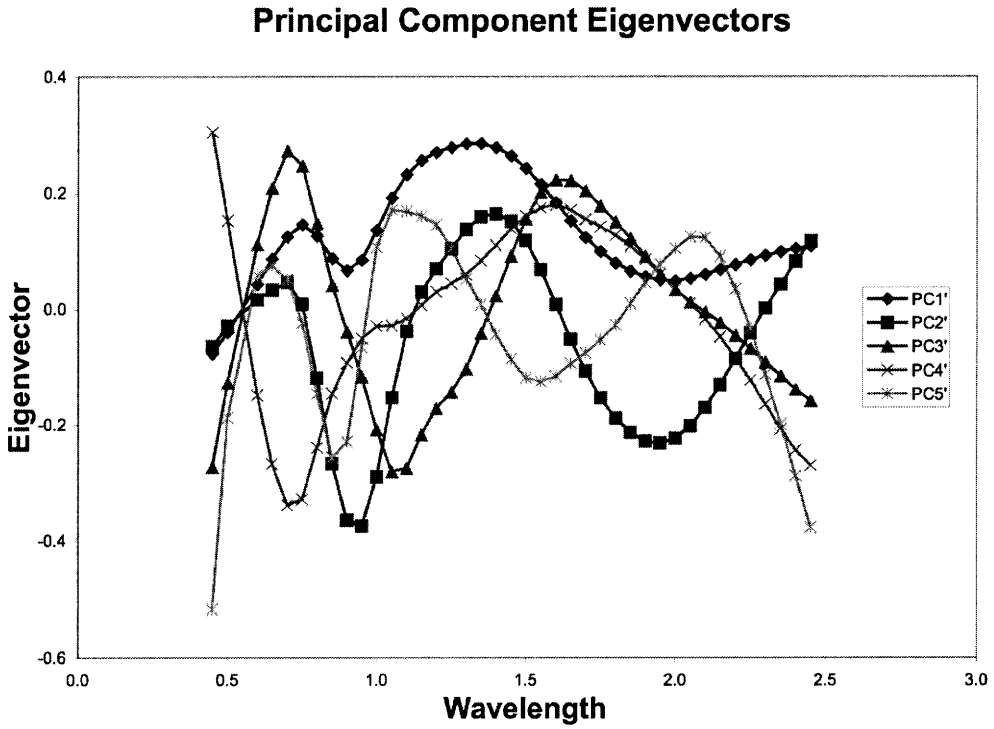

Figure 5: Sensitivity of Principal Components over wavelength range. High positive or negative values indicate that a principal component is more sensitive to information over that region. This figure shows that PC4' and PC5' are more sensitive to features at the ends of the spectrum, while the others are more sensitive to features in the middle.

3.3.3 Choosing the right number of Principal Components

Bus used slope plus three principal components to characterize his visible data. Because data in the extended wavelength range have many more features we use slope plus 5 principal components. We look at the amount of variance contained within each principal component to determine how many to use. Greater variance means more information is contained within that principal component.

Because 40 channels were put into PCA, 40 principal components were the output. Since PCA puts the most information in the first dimensions, and decreases with

each successive dimension, we only want to look at some of the principal components. To decide how many principal components we want to use in our analysis we must look at the variance contained within each. Table 1 shows percentage variance contained within each principal component. Note that slope is not included in this calculation, so this percentage represents the variance left over after the slope was removed. PC10' through PC40' contribute essentially no new information so are therefore not included in the table. Upon inspection we see that most of the variance exists in the first six principal components. Figure 6 shows a scree plot of the variance. Scree is rubble rock at the bottom of a mountain. On scree plot the point where the plot levels off after the drop determines at which principal component to stop. (Jackson 1993) We see the chart level off around PC5' and PC6'. We decided that since 99.2% of the variance was contained within the first 5 principal components, they were sufficient. It is evident that PC5' does not seem to contain a significant amount of information, however, we found it useful for classifying C-complex objects. By running PCA with the slope included in the data we found that slope accounts for 88.4% of all the variance within the data. All the other principal components combined account for 11.6%. Slope plus the first five PC' account for 99.9% of the variance. Table 2 shows the variances accounted for by the slope plus the first five principal components.

Table 1 Variance Contained within Each Principal Component (not including slope)

We find 99.2% of the variance is accounted for by using PC1' through PC5'

Principal Component	Variance (%)
PC1'	63.1
PC2'	24.3
PC3'	8.9
PC4'	2.2
PC5'	0.6
PC6'	0.3
PC7'	0.2
PC8'	0.1
PC9'	0.1
PC10'-PC40'	0.1
Total:	100.0

Table 2 Variance Contained within Slope and Principal Components

PC	Variance (%)
Slope	88.4
PC1'	7.3
PC2'	2.8
PC3'	1.0
PC4'	0.3
PC5'	0.1
Total:	99.9

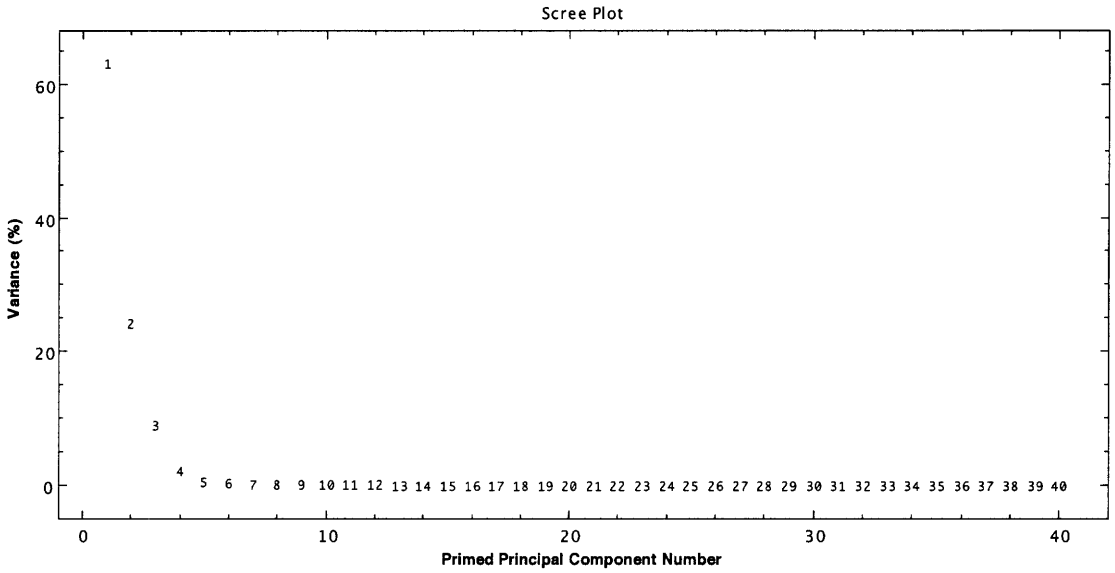

Figure 6: Scree Plot. This plot shows the amount of variance contained in each principal component. The further down in principal component space, the less information is contained in each principal component. PC1' through PC5' contain most of the variance in the data set. Notice that PC5' lies just at the bottom of the downward slope indicating it is a good place to stop using components. (Jackson 1993)

3.3.4 A Note on Notation: What is the difference between PC1' and PC1?

If the original, normalized and splined data without the slope removed were analyzed with PCA the first transformation would be PC1. PC1 corresponds to slope. However, we remove the slope and re-perform PCA. In this case, we denote the slope-free PCA results as PC1', PC2', etc. We use the " ' " notation so as to recall that PC1' is closely analogous to PC2 in the original (no slope removed) data set.

4. The Taxonomy

The most striking feature plotted from the principal components is the large gap in PC1' versus PC2' space seen in Figures 7 and 8. It appears that this clear boundary distinguishes between spectra that have a two micron absorption band and those that don't. This gap is well represented by the line:

$$PC1' = -3.00PC2' - 0.28 \qquad (\text{line } \alpha) \qquad (1)$$

All objects below and to the left of this line have no two micron absorption features and include all featureless (C, X complex) spectra. Objects plotted to the right of and above the line have two micron absorption features, and farther right signifies stronger absorption. Moving right in the orthogonal direction to line α also seems to signify narrowing 1 micron bands. For example, V-types plot furthest to the right. The only classes that cross this gap are the A and Sa classes. Interestingly the K-class, long considered as an intermediate between S and C, falls most squarely in the gap. Figures 7 and 8 plot all objects in PC1' and PC2' space. Figure 7 shows the objects plotted with original Bus labels, while Figure 8 shows the new DeMeo labels. An enlargement of the gap present at line α is shown in Figure 9.

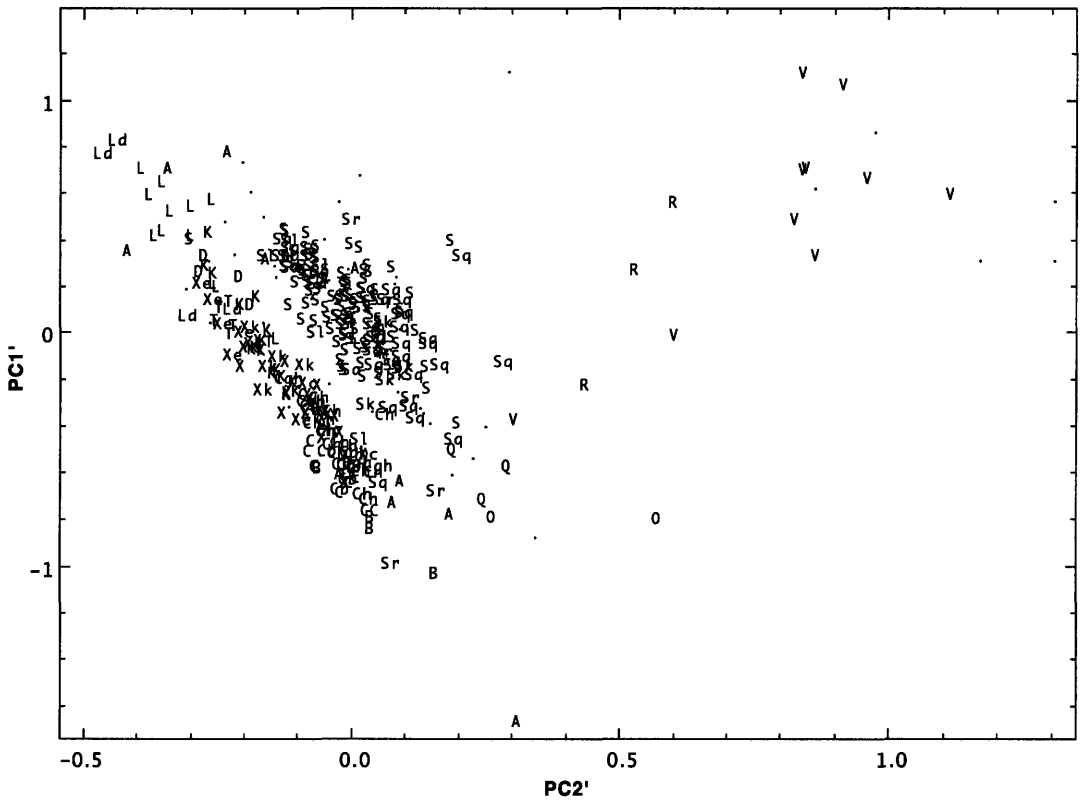

Figure 7: Plot of PC1' versus PC2' for all objects. These objects are plotted with their original labels under the Bus system. Objects that do not have Bus designations are labeled as a ".".

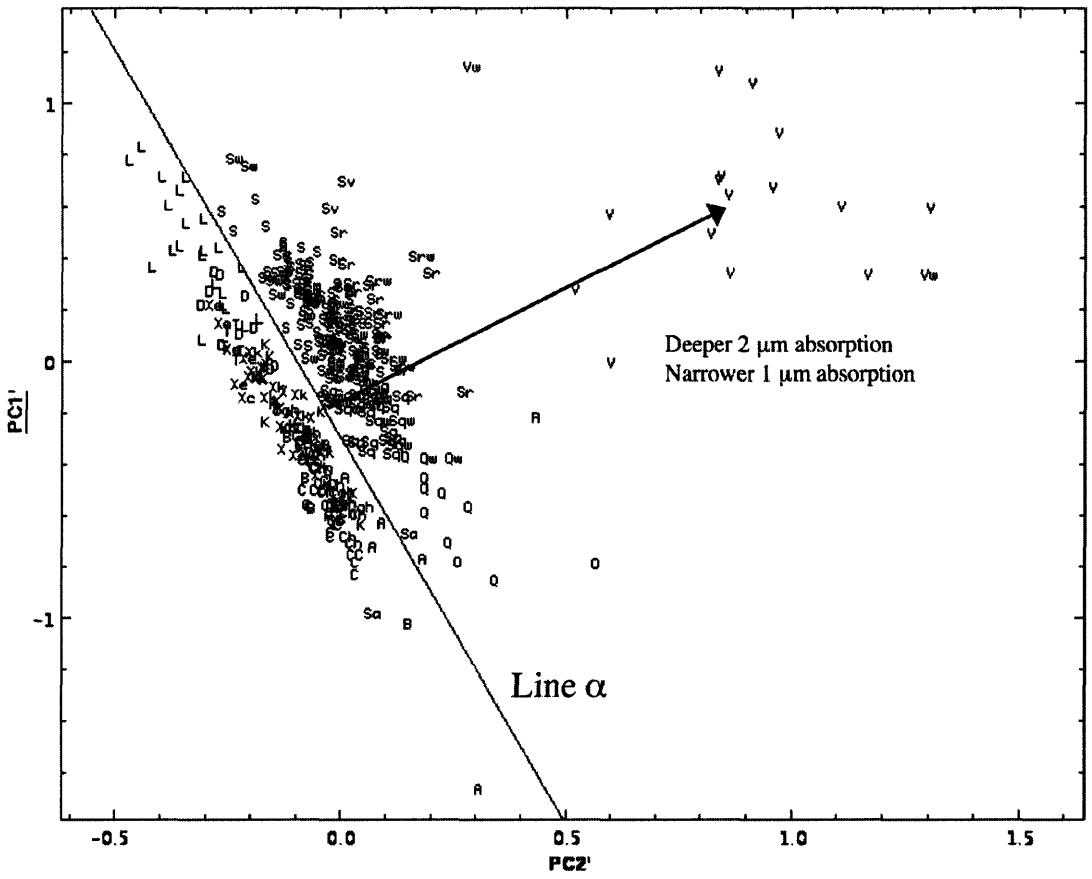

Figure 8: Plot of PC2' versus PC1'. All objects plotted are labeled with their DeMeo taxonomy classification. Notice the large gap between the S-complex and the C- and X-complexes. Line α separates objects with and without 2 μm absorption bands. The direction orthogonal to line α indicates deeper 2 μm and narrower 1 μm absorption bands.

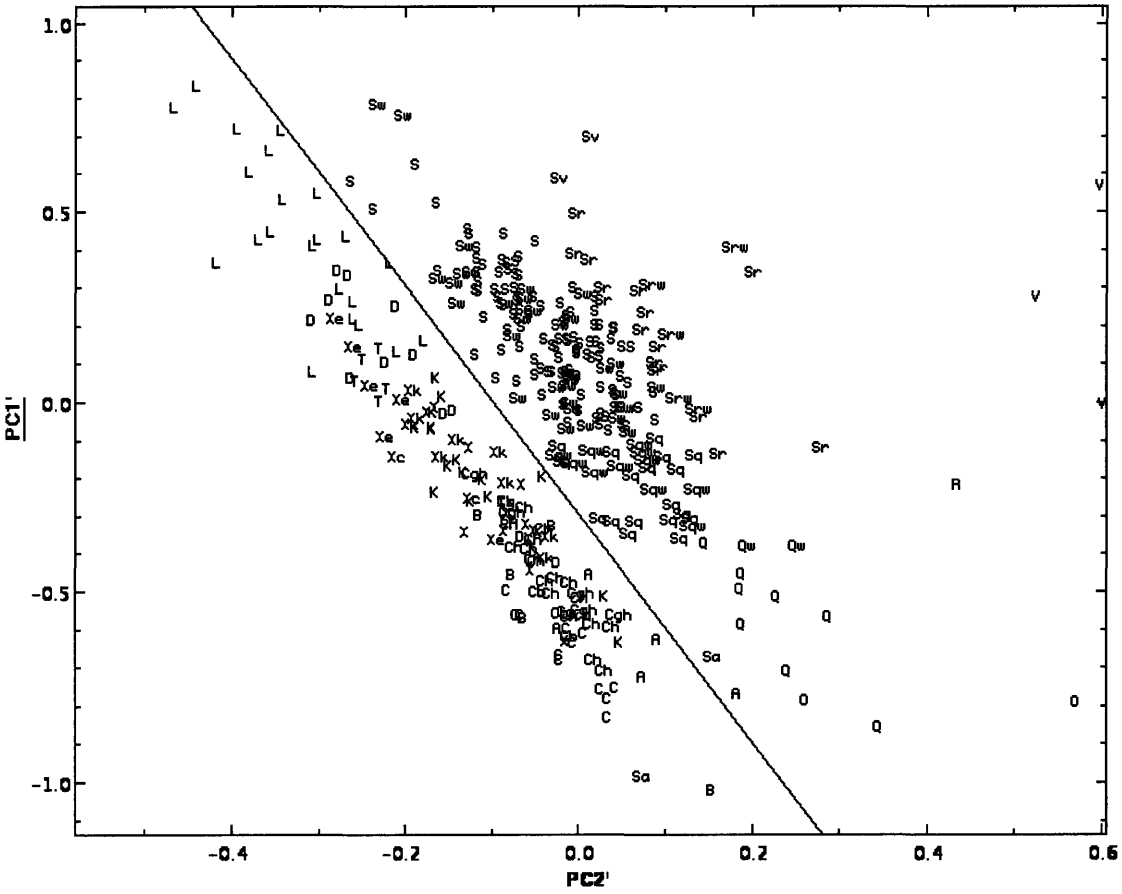

Figure 9: Enlargement of gap in PC1' and PC2' space. This figure shows the clear distinction between the S-Complex and end members with 2 μm absorption bands and objects that are featureless or have only 1 μm absorption bands.

In defining classes for the taxonomy we created a flowchart (Appendix D) containing steps to find the right combination of principal components ranges that result in the correct class for each object. The order of the flow chart is significant because some classes overlap in certain principal components but can be separated in others. For all the new labels to the 365 objects in the dataset see Appendix E. We start by separating the A and Sa classes because they cross over the large gap in PC1' and PC2' space. The DeMeo Sa class was relabeled from the Bus system because the two Sa objects in this system were both Sr-types in the Bus system. Since these objects prove to

be intermediate between S and A change the name of these two Sr-types. This is step 1 in the flow chart. Refer to Appendix C for the complete chart. Figure 10 shows the progression from S to Sa to A type.

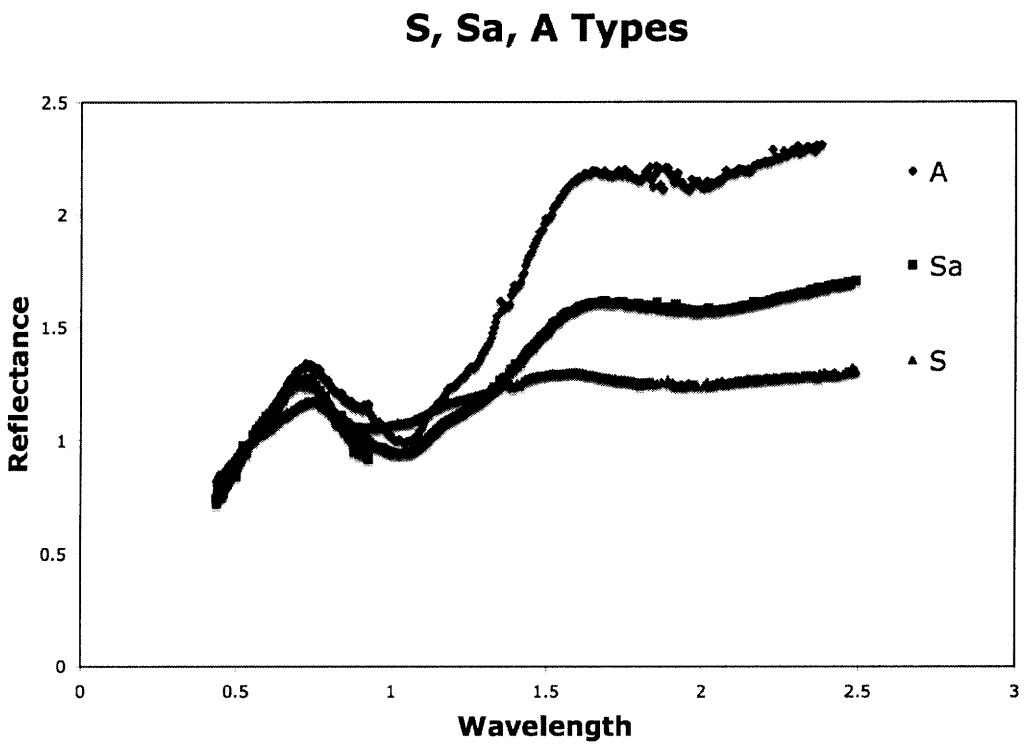

Figure 10: Plot of S, Sa, and A. There is a clear progression from S with a shallow one micron band and low slope to A with a deep one micron band and high slope. Sr seem to to resemble A-type one micron band absorption very well, but are much less red than A-types.

Step two starts by separating all objects by the divide (line α) in PC1' versus PC2' space. Step two continues to create boundaries for objects with a two micron band and step three addresses featureless objects (the C- and X-complexes) as well as K and L classes which have no significant two micron band.

We started by looking at the end member classes in PCA space since they separate more clearly making them the easiest to define. In Figure 10 you can see the data of Figure 8 with lines separating S-complex and end member classes. The V class lies to the right of the line parallel to line α noted as equation 2:

$$PC1' = -3.0PC2' + 1.5 \qquad \text{(line } \delta\text{)} \qquad (2)$$

The R class lies to the left of line δ but right of equation 3 and above equation 4:

$$PC1' = -3.0PC2' + 1.0 \qquad \text{(line } \gamma\text{)} \qquad (3)$$

$$PC1' = 1/3PC2' - 0.4 \qquad \text{(line } \eta\text{)} \qquad (4)$$

To see the lines labeled in PCA space refer to Figure 11. Note that there is only one R-type object in our sample, 349 Demboska, for which the class was created. Also, there are only two O-type objects among our data. Even though the class is separated in the flow chart, more data on R-type and O-type objects may change the region boundaries significantly. To see the differences between the end member classes V, R, Q, and O see Figure 12.

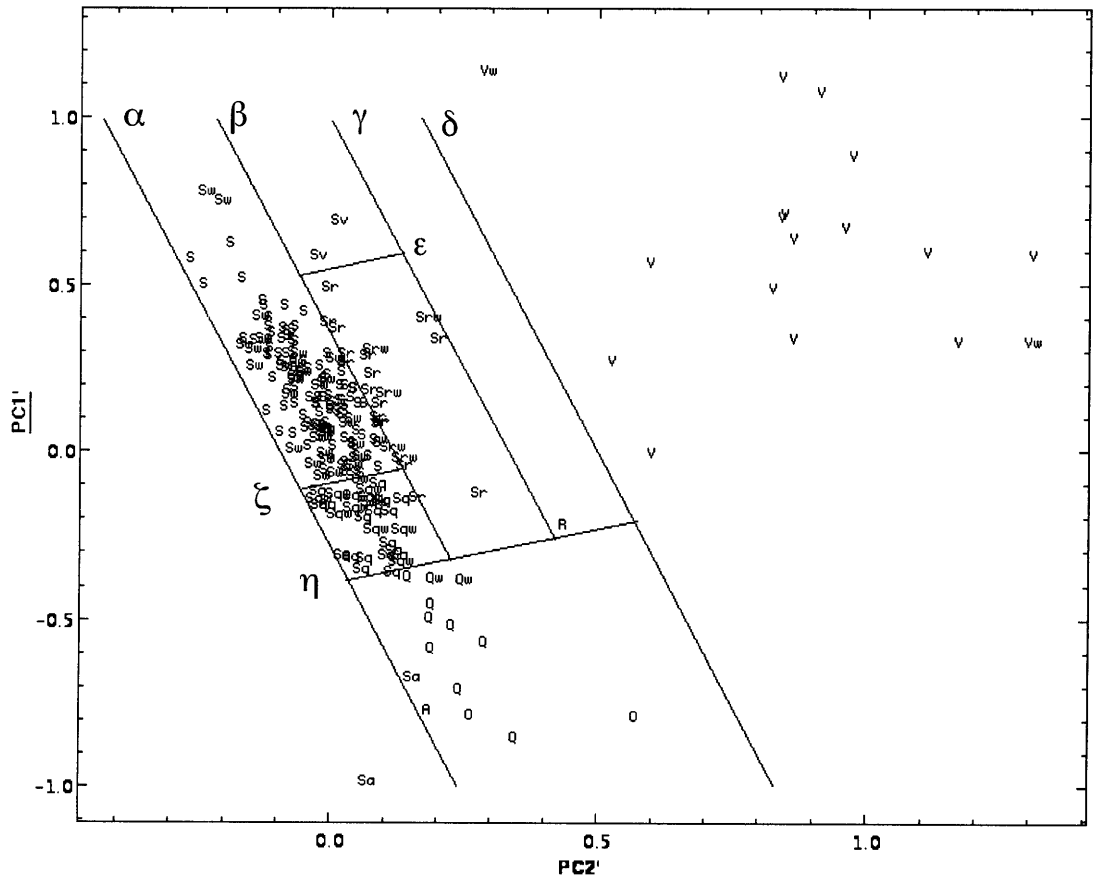

Figure 11: Plot of PC2' vs. PC1'. This plot shows the lines that divide the objects with and without 2 micron absorption bands, as well as the V and R class boundaries.

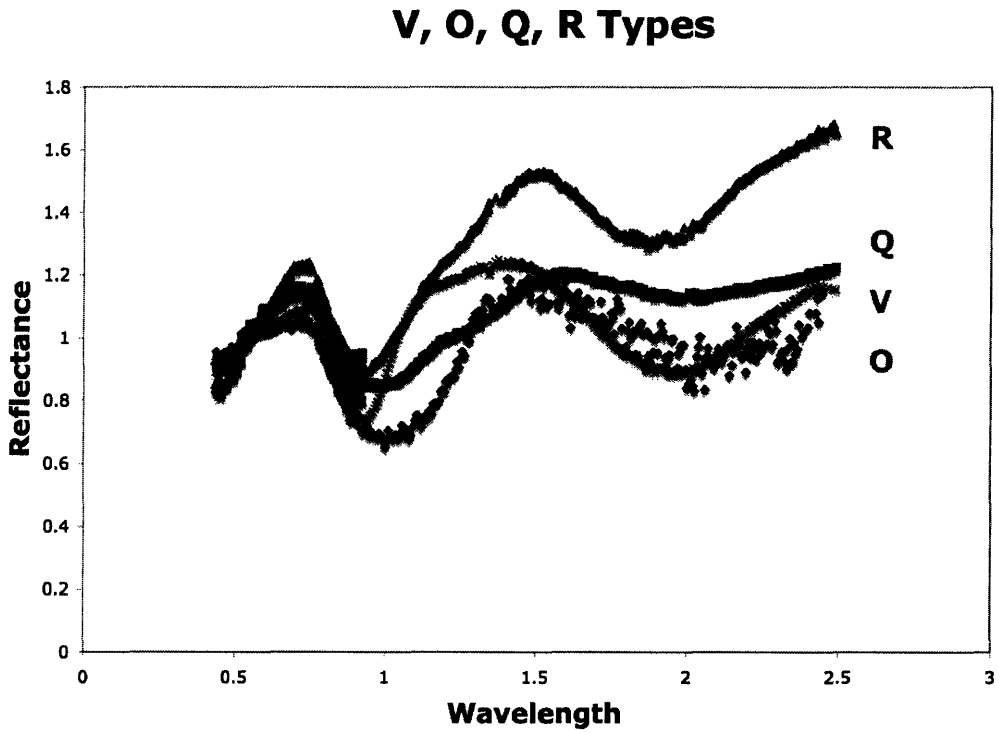

Figure 12: Plot of V, O, Q, R Types. This plot shows typical spectra in each end member class. Note O has a very wide 1 micron band and V has a very narrow band. The V-types with the deepest 2 micron bands plot farthest from line α.

The S-complex was by far the most difficult to define. Most classes seemed to blend together or scatter randomly in all combinations of PCA components. Sa and Sl (named under the Bus taxonomy) were entirely indistinguishable so the Sl class was combined. Sa objects were most easily distinguishable not by absorption features, but by their greater slope (caused by slope increases in the 1 to 1.5 micron range.) The S, Sq, and Sk objects were initially impossible to define clearly because the boundaries seemed to blur and overlap. We performed a new principal component analysis to help guide us.

Because the main difference between the S-classes appears to be the width of the 1 micron absorption band we used the wavelength range 0.8 to 1.35 microns and did PCA on only S-type objects. Sa types were scattered randomly supporting that their main difference is slope. From this new PCA (sPCA) we found that sPC1 and sPC2 best separated the classes. We relabeled objects based on sPCA and plotted the newly changed labels back in the original PCA.

Once we used sPCA to guide our labels, we could use PC1' and PC2' to create definitions within our original principal components. We continued to use boundaries parallel and perpendicular to line α. Each class has its own box in PC1' and PC2' space. Refer to Figure 13 to see the S-complex boxes labeled in PCA space. The S class was right of line α (equation 1), to the left of equation 5 and above equation 6.

$$PC1' = -3.0PC2' + 0.35 \qquad (\text{line } \beta) \qquad (5)$$

$$PC1' = 1/3PC2' - 0.10 \qquad (\text{line } \zeta) \qquad (6)$$

Objects that reside below line ζ (equation 6) appear similar to Q-types, but with more shallow absorption bands. These are Sq-types transitioning between S and Q. They lie right of line α, left of line β, below line ζ, which is the S-type boundary, but above line η, which is the boundary for Q-types. Sr-types transition between S and R classes. They reside between lines β and γ, and between lines η and ε given in equation 7.

$$PC1' = 1/3PC2' + 0.55 \qquad (\text{line } \varepsilon) \qquad (7)$$

The objects between β and γ, but above line ε were unique from Sr because they exhibited very narrow 1 μm absorption bands. These two objects appear to transition between S and V classes. They are not included in the Bus dataset, and Bus (1999) did

not report any cases of these objects. They are given the label Sv. The Sk type was non-unique and was absorbed into the other S classes

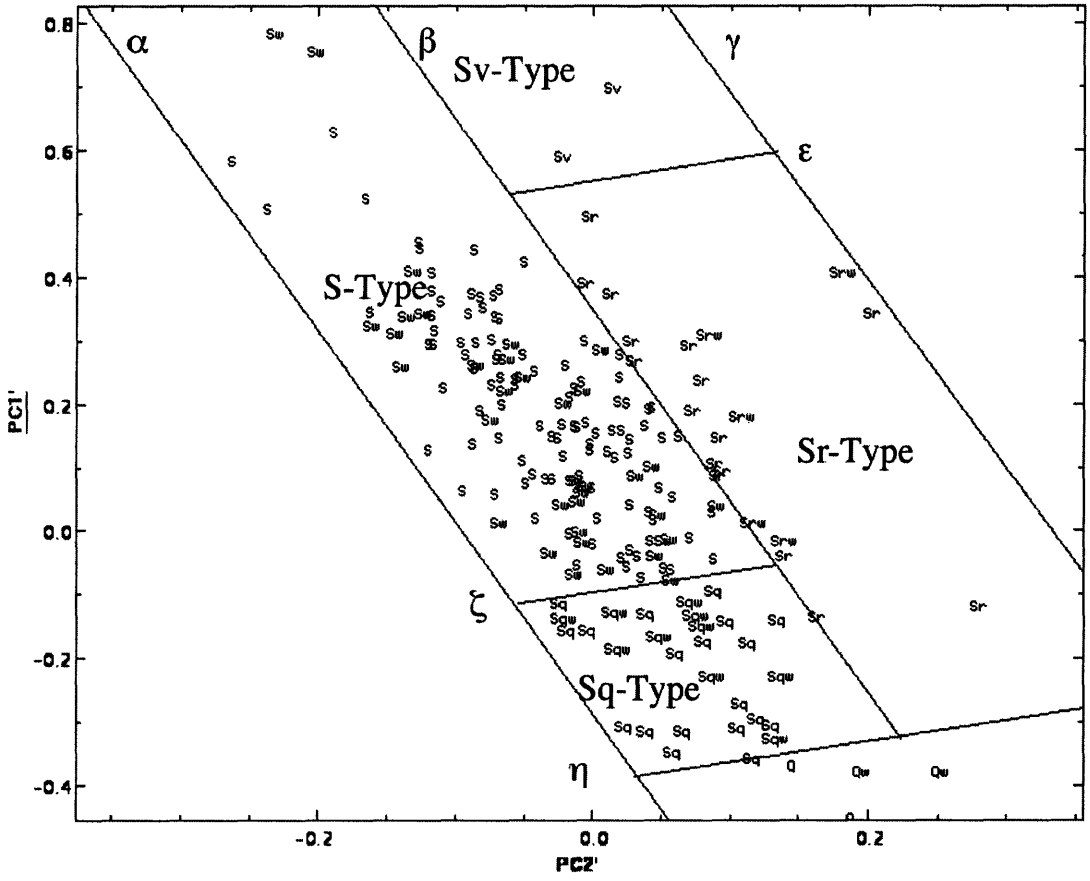

Figure 13: PC2' versus PC1' plotted for the S-complex. Each class has its unique box bounding it. All lines are perpendicular or parallel to line α.

Sa and Sl (labeled under the Bus system) objects were indistinguishable when extending to the near-infrared. Their features were also indistinguishable from other S-complex objects, and it seems that their slope was the major distinction. Because the Sa and Sl designations did not indicate that these objects were intermediate classes between

S and A or L we felt that the notation was misleading. We removed the Sa and Sl designations given by Bus and replaced them by designations of S, Sq, Sr, and Sv based on PC1' and PC2' which represented absorption features. We felt, however, that even though slope did not merit a class distinction, it was worth noting in the taxonomy.

The S, Sq, and Sr classes all had very widely varying slopes. High slopes are indicative reddening by space weathering (Clark et al. 2002). Even though slope has no mineralogical significance we thought it fitting to distinguish between objects that had undergone significant space weathering from those who had not. We made a cutoff, albeit an arbitrary one, at Slope = 0.25 dividing "high slope" objects from other objects. These objects are not relabeled in a class of their own. Instead the S, Sk, and Sq objects with high slopes get a notation of "w" added to their name to indicate a "weathered" object. The high slope S objects are labeled Sw, Skw, and Sqw. There were also two V-type objects and two Q-types with slopes greater than 0.25, which were labeled Vw and Qw. To see the difference between a low and high slope object, S and Sw, refer to Figure 14.

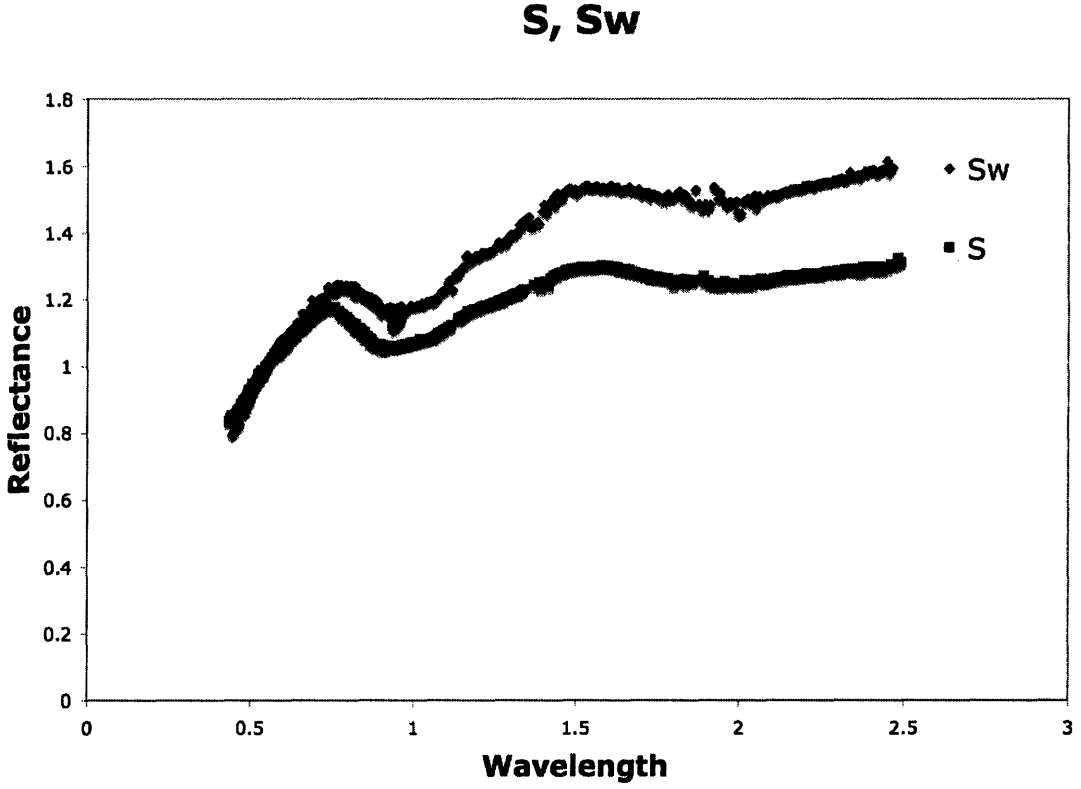

Figure 14: Plot of S and Sw. The absorption features for both are very similar. Slope is the most significant distinction between the two.

The choice of 0.25 for the slope cutoff was somewhat arbitrary. When plotting Bus labeled S, Sa, and Sl objects, there was a mixing around the 0.23 to 0.27 slope range. We wanted to keep the "w" notation more selective, but also didn't want to set the cutoff too high where objects with unusual slope features (such as deeper UV dropoffs) were preferentially selected rather than focusing on the significant slope range between one and two microns for the S-Complex. See Figure 15 for the plot of Slope versus PC1' that shows the line separating weathered objects from regular objects.

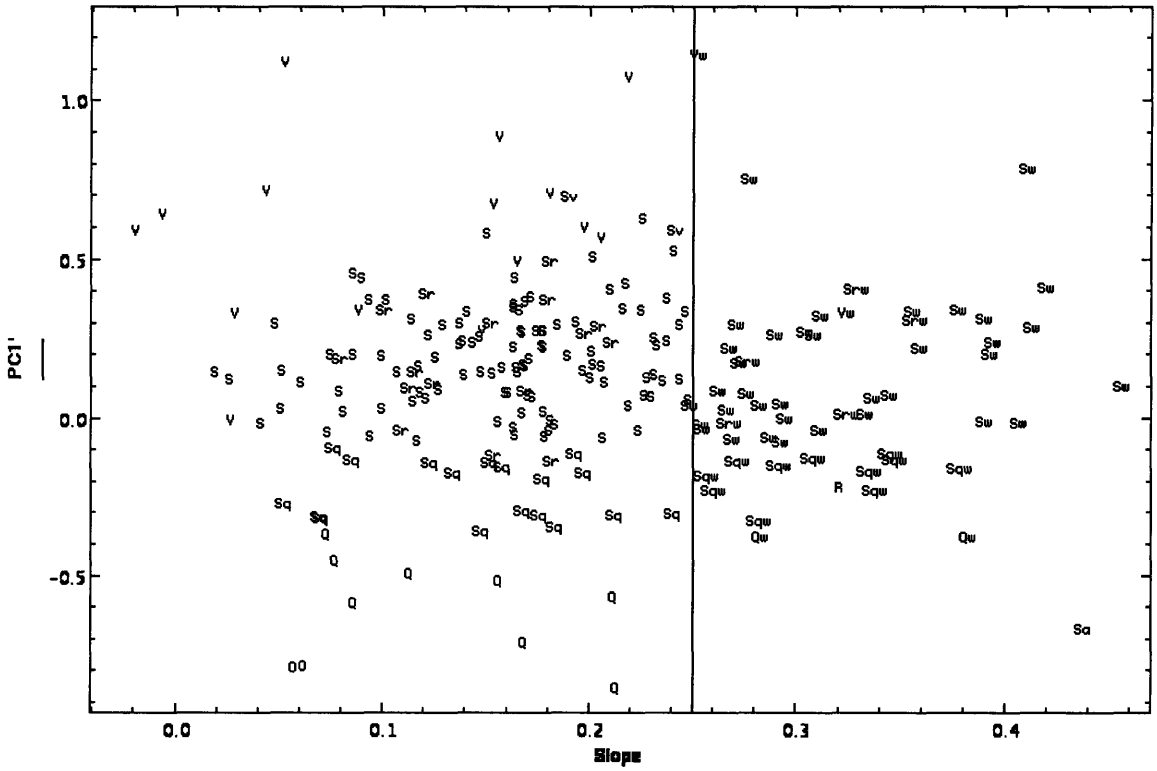

Figure 15: Plot of Slope versus PC1' for the S-Complex. All objects with slopes greater than 0.25, regardless of their subclass (S, Sq, Sk), get a "w" notation indicating weathering. Note the two V and Q class objects labeled "Vw" and "Qw." Dembowska, as the only R member, does not get a w.

Step three focused on objects below or to the left of line α (equation 1). We again start by removing end members. D and T classes are easily separated by their high slopes and PC1', PC2', and PC3' values. Next, we separate out L objects based on the PC2' versus PC1' plot. When an object fits in the L component space it is necessary to check for Xe type objects. Xe is a class defined in the Bus system that has a distinct hook at 0.49 microns. By visually inspecting the spectrum, one can notice the presence of a

feature at 0.49 and an absence of a slight feature around 1 micron and label the object an Xe instead of an L. Refer to Figure 16 to see Slope versus PC1' which shows how D, L, and L are fairly distinct. The K types can then be distinguished clearly in PC2' and PC3' space. We found that all Ld type objects under the Bus system could be fit in either the L or D classes when near-infrared data were added. Since it is not necessary for distinguishing classes, it was removed from the DeMeo system. Figure 17 shows how the K class is distinct.

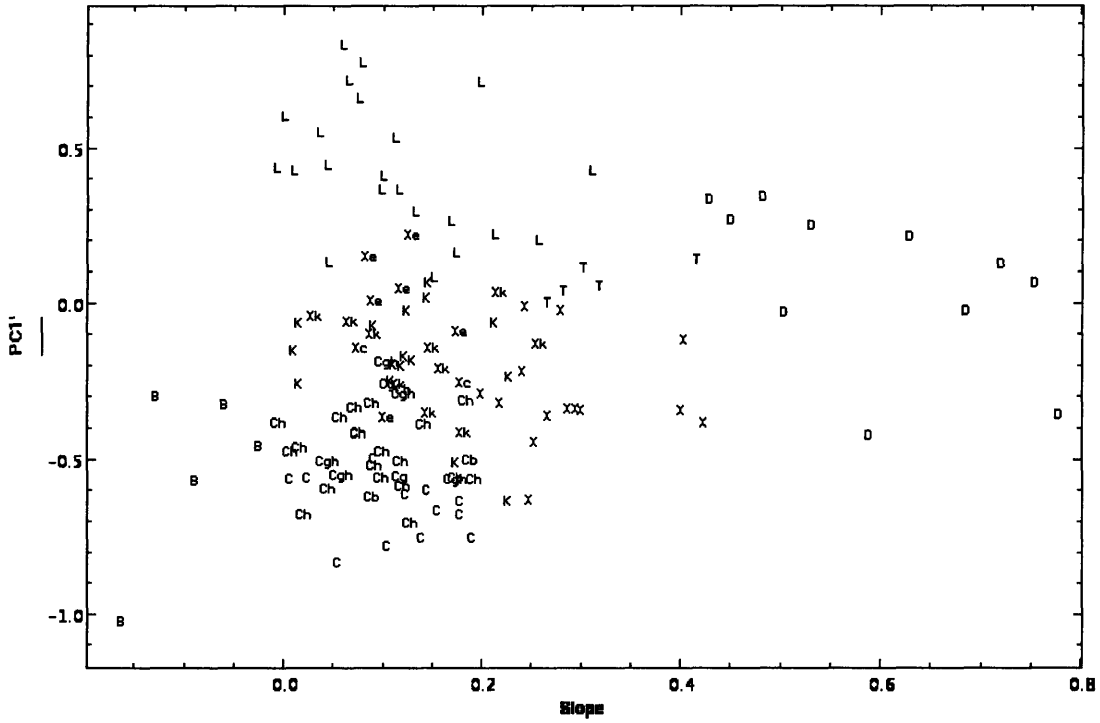

Figure 16: Plot of Slope v. PC1'. Note how D, T, and L are fairly distinct in this component space. K separates better in PC2' and PC3' space.

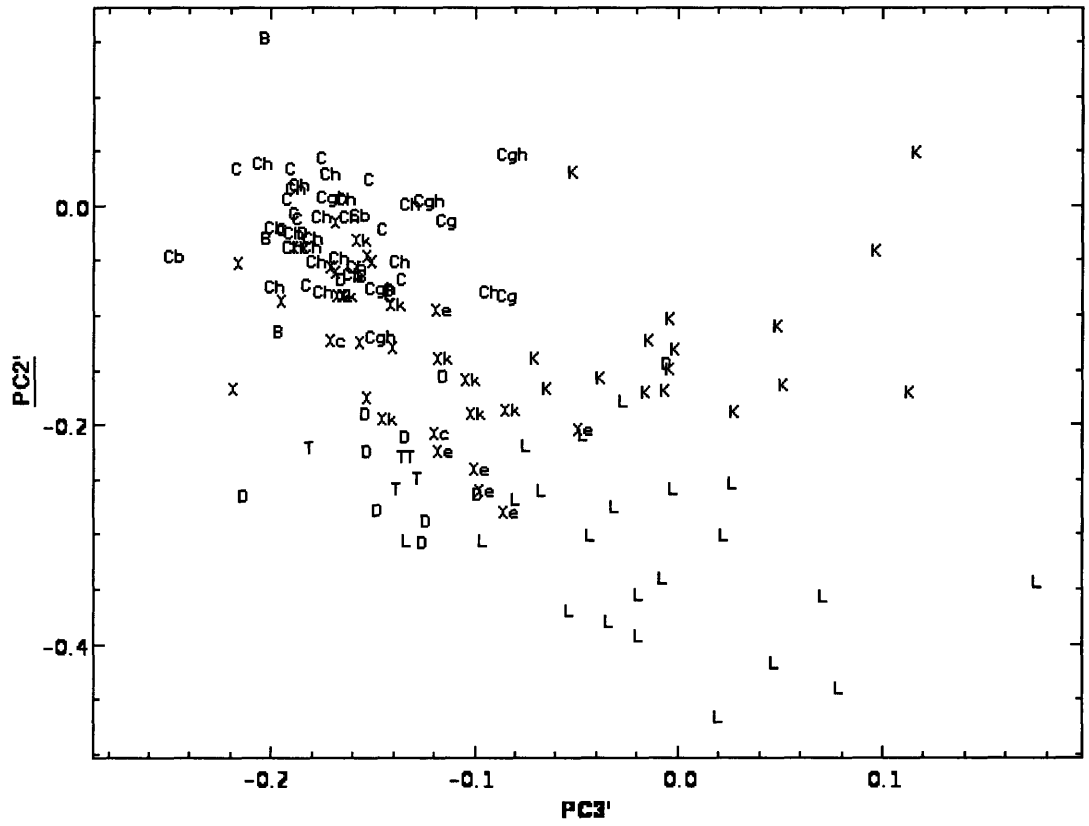

Figure 17: Plot of PC3' v. PC2'. The K types are distinct in this component space.

This brings us to the X and C complexes. The B-types are easily distinguished by their negative slope as well as negative PC1' and PC4' values. The X-class can then be easily removed based on high slope values between 0.2 and 0.425. At this point Xk objects may be in X-class PC' space. When visually inspecting the spectrum if there is a feature present at 1 micron, the object is designated an Xk. Figure 18 shows a plot of the C- and X- complexes.

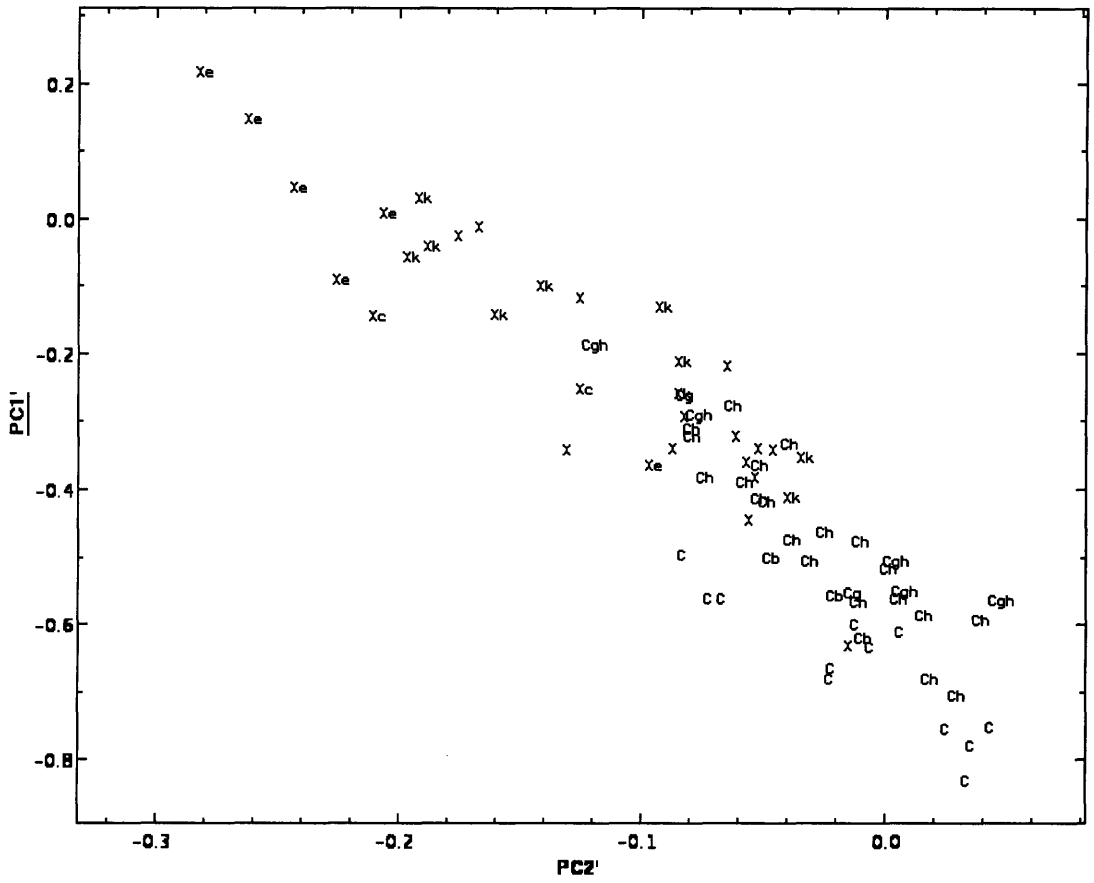

Figure 18: Plot of PC2' v. PC1' for the C- and X-Complex. These components help separate the two complexes. Slope will also differentiate the two.

The Ch objects are defined well in PC1' and PC4' space, but a check must be done to see if a strong 0.7 micron feature exists, making the object a Cgh. The C and Cb types separate in PC1', PC4', and PC5'. See Figure 19 and 20 to see the C-complex plotted in PCA space. After this the Cgh, Ch, Xk, Xc, and Xe types don't all separate cleanly in component space and are heavily dependent on visually detecting features.

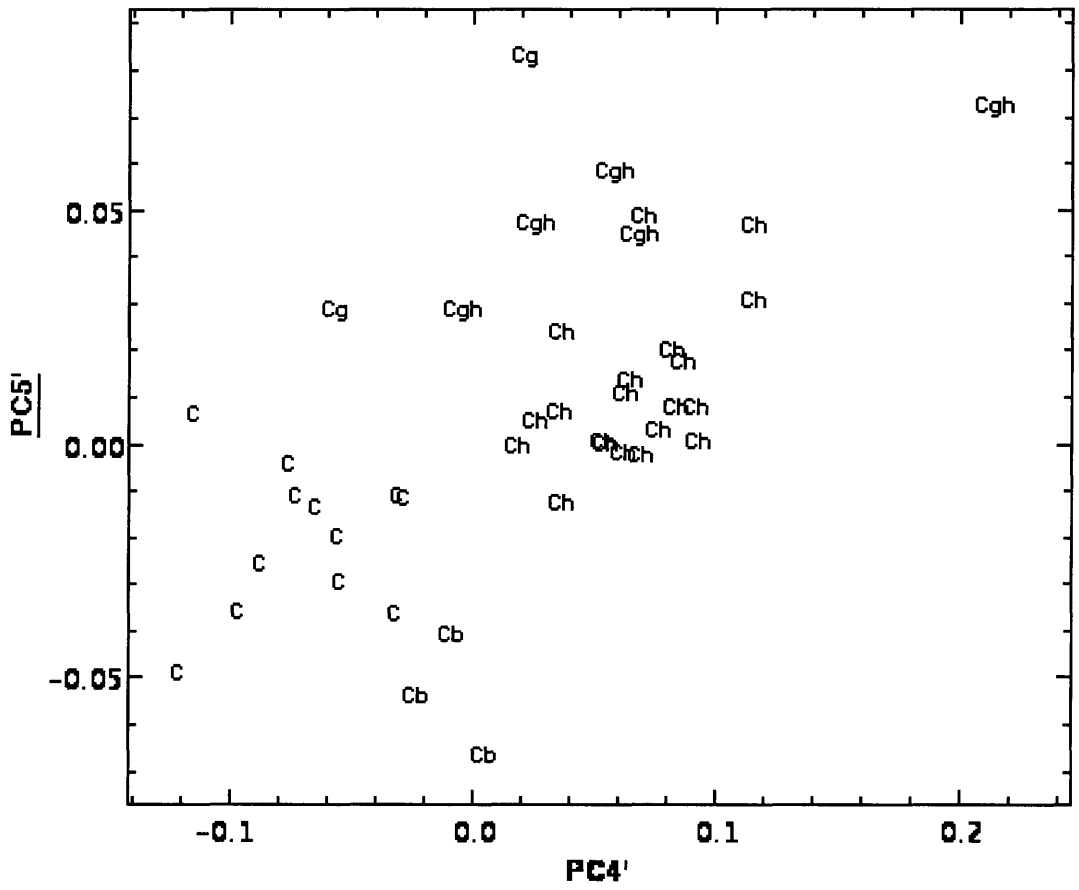

Figure 19: Plot of PC4' v. PC5' for C-Complex. The classes are easily distinguishable in this component space.

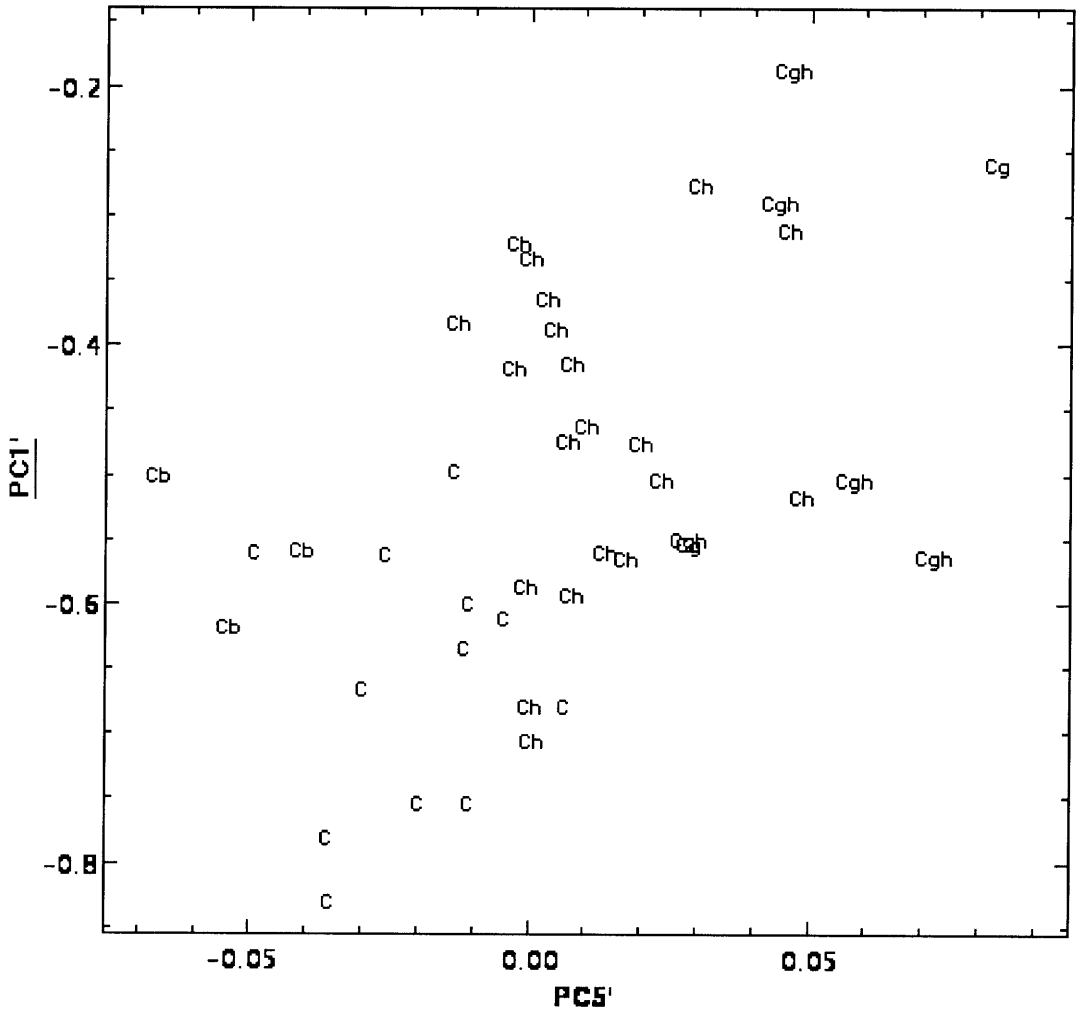

Figure 20: Plot of PC5' v. PC1'. A second plot demonstrating the separation among C-types.

We currently do not have a method for classifying spectra using only near-infrared data because putting reflectance values into the eigenvectors from this work would be meaningless since the entire range doesn't exist. In future work we hope to include a method for using near-infrared only data to find a taxonomic classification. However

note: certain classes evolve unchanged from the Bus taxonomy that are based on features measured at visible wavelengths. Assignment to these classes (Cg, Cgh, Xc, Xe, Xk) therefore requires visible wavelength data.

5. Conclusion

A new taxonomy with was created using Principal Component Analysis and visible features to characterize visible and near-infrared wavelength spectral reflectance values. The system, based on the Bus visible taxonomy from Bus (1999), has 24 classes compared to 26 in the Bus system. The changes in classes are summarized in Appendix A. We used all of the seven possible changes from the previous system to the new highlighted in Figure 3. We eliminated three classes: Ld, Sl, and Sk. All the S subclasses (Sa, Sl, Sk, Sq, Sr) had objects that merged back into the S class, although many Sq objects remained Sq and two Sr objects were relabeled Sa. A new intermediate class, the Sv class, was created to branch the S and V classes. High-sloped S, Sa, Sq, Sr, V and Q objects were given a "w" notation to indicate weathering. Many of the classes that lie left of line α are either featureless or exhibit only small features at visible wavelengths identified by Bus (1999). It is still necessary to use these visible features to distinguish the classes because there are no other distinguishing features at near-infrared wavelengths. 365 objects were given types based on the DeMeo taxonomic system which was created using 6 dimensions including Slope and PC1' through PC5' of Principal Component Analysis.

References

Barucci, M.A, Capria, M.T., Coradini, A., Fulchignoni, M. (1987). Classification of asteroids using G-mode analysis. Icarus 72, 304-324.

Binzel, R.P., Xu, S. (1993). Chips off of asteroid 4 Vesta: Evidence for the parent body of basaltic achondrite meteorites. Science 260, 186-191.

Binzel, R.P., Rivkin, A.S., Stuart, J.S., Harris, A.W., Bus, S.J., Burbine, T.H., (2004). Observed spectral properties of near-Earth objects: results for population distribution, source regions, and space weathering processes. Icarus 170, 259-294.

Bowell, E., Chapman, C.R., Gradie, J.C., Morrison, D., Zellner, B. (1978). Taxonomy of Asteroids. Icarus 35, 313-335.

Bus, S.J., (1999). *Compositional structure in the asteroid belt: results of a spectroscopic survey.* Doctoral thesis. Massachusetts Institute of Technology, Cambridge, Massachusetts.

Bus, S.J., Binzel, R.P., (2002). Phase II of the Small Main-Belt Asteroid Spectroscopic Survey. Icarus 152, 106-145.

Chapman, C.R., Johnson, T.V. (1971). A review of spectrophotometric study of asteroids. Physical Studies of Minor Planets (T. Gehrels, Ed.), 51-65. NASA SP-267.

Chapman, C.R., Morrison, D., Zellner, B., (1975). Surface properties of asteroids: A synthesis of polarimetry, radiometry, and spectrophotometry. Icarus 25, 104-130.

Clark, B.E., Hapke, B., Pieters, C., Britt, D. (2002) Asteroid Space Weathering and Regolith Evolution. In *Asteroids III*, (W.F. Bottke, A. Cellino, P. Paolicchi, R.P. Binzel eds.), Univ. Arizona Press, 585-599.

Consulmagno, G.J., Drake, M.J. (1977). Composition and evolution of the eucrite parent body – Evidence from rare earth elements. Geochimica et cosmochimica Acta. Vol 41 Isssue 9, 1271-1282

DeMeo, F.E., Binzel R.P (2007). Comets in the near-Earth Object Population. Icarus. Submitted for publication.

Gaffey, M.J., Bell, J.F., Brown, J.R., Burbine, T.H, Platek, J.L., Reed, K.L., Chaky, D.A., (1993). Mineralogic Variations within the S-Type Asteroid Class. Icarus 106, 573-602.

Jackson, D.A. (1993) Stopping rules in Principal Component Analysis: A comparison of heuristical and statistical approaches. Ecology 74 2202-2214.

Rayner, J.T., Toomey, D.W., Onaka, P.M., Denault, A.J., Stahlberger, W.E., Vacca, W.E., Cushing, M.C., Wang, S. (2003) SpeX: A medium-resolution 0.8-5.5 micron spectrograph and imager for the NASA Infrared Telescope Facility. Astron. Soc. of the Pacific 115 362-382.

Tholen, D.J. (1984) *Asteroid taxonomy from cluster analysis of photometry.* Doctoral Thesis, University of Arizona.

Tholen, D.J., Barucci, M.A. (1989) Asteroid taxonomy. In *Asteroids II* (R.P.Binzel, T.Gehrels, and M.S. Matthews, Eds.), 298-315. Univ. of Arizona Press.

Tody, D. (1993). IRAF in the Nineties. In Astronomical *Data Analysis Software and Systems II* (R. J. V. Brissenden, and J. Barnes, Eds.), pp 173. Astron. Soc. of the Pacific, San Francisco.

Wood, J.H. Kuiper, G.P (1963) Photometric studies of asteroids. Astrophys. J. 137, 1279-1285.

Vernazza, P., Birlan, M., Rossi, A., Dotto, E., Nesvorny, D., Brunetto, R., Fornasier, S., Fulchignoni, M., Renner, S. (2006) Physical characterization of the Karin Family. AA 460, 945-951

Appendix A: Bus-DeMeo class changes

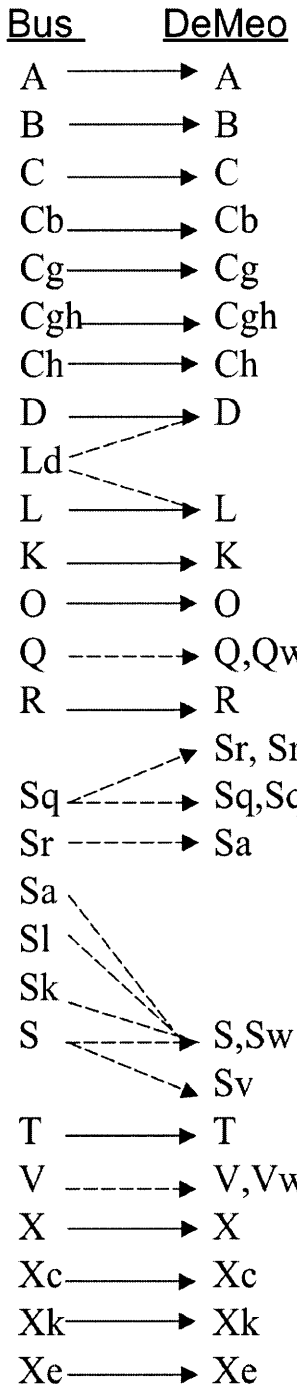

Total:	26	24

Eliminated: Ld, Sk, Sl

Created: Sv

w notation does not denote a distinct class.

Appendix B: Observation List

Object	Obs Date	Telescope	Object	Obs Date	Telescope
1	19-May-05	IRTF 3m	65	30-Sep-03	IRTF 3m
2	29-Mar-01	IRTF 3m	66	22-Nov-05	IRTF 3m
3	17-Mar-03	IRTF 3m	67	16-Jun-04	IRTF 3m
4	9-Oct-00	IRTF 3m	69	11-May-05	IRTF 3m
5	20-Feb-04	IRTF 3m	70	29-Sep-02	IRTF 3m
7	20-Feb-04	IRTF 3m	73	16-Oct-03	IRTF 3m
8	16-Sep-02	IRTF 3m	76	5-Sep-05	IRTF 3m
10	19-Feb-04	IRTF 3m	77	25-Oct-06	IRTF 3m
11	13-Nov-05	IRTF 3m	78	31-Oct-05	IRTF 3m
13	19-May-05	IRTF 3m	82	24-Aug-01	IRTF 3m
14	17-May-01	KPNO 4m	84	2-Aug-03	IRTF 3m
15	17-Aug-02	IRTF 3m	85	2-Aug-03	IRTF 3m
16	21-Jan-07	IRTF 3m	87	4-Sep-05	IRTF 3m
17	15-Aug-01	IRTF 3m	90	5-Sep-05	IRTF 3m
18	22-Jun-01	IRTF 3m	92	8-Oct-00	IRTF 3m
19	29-Jan-06	IRTF 3m	93	27-Apr-03	IRTF 3m
20	22-Jun-01	IRTF 3m	96	28-Jan-06	IRTF 3m
21	22-Sep-04	IRTF 3m	97	8-Oct-05	IRTF 3m
22	25-Oct-06	IRTF 3m	99	13-Nov-05	IRTF 3m
24	8-Oct-05	IRTF 3m	101	22-Dec-06	IRTF 3m
25	30-Jan-01	IRTF 3m	103	14-Aug-01	IRTF 3m
26	24-Aug-01	IRTF 3m	105	2-Aug-03	IRTF 3m
27	1-Jun-02	IRTF 3m	106	2-Aug-03	IRTF 3m
28	13-Jan-02	IRTF 3m	108	31-May-02	IRTF 3m
29	29-Jan-01	IRTF 3m	110	29-Jan-01	IRTF 3m
30	8-Oct-00	IRTF 3m	111	22-Sep-04	IRTF 3m
32	30-Jan-01	IRTF 3m	114	28-Jun-06	IRTF 3m
33	6-Mar-02	IRTF 3m	115	6-Mar-02	IRTF 3m
34	20-Feb-04	IRTF 3m	119	21-Jun-01	IRTF 3m
37	15-Aug-01	IRTF 3m	128	2-Aug-03	IRTF 3m
38	5-Jul-03	IRTF 3m	130	29-Mar-01	IRTF 3m
39	14-Aug-01	IRTF 3m	131	20-Jul-06	IRTF 3m
40	16-Oct-04	IRTF 3m	132	5-Sep-05	IRTF 3m
41	15-Sep-04	IRTF 3m	133	22-Jun-01	IRTF 3m
42	21-Jun-01	IRTF 3m	147	2-Aug-03	IRTF 3m
43	22-Nov-05	IRTF 3m	150	2-Aug-03	IRTF 3m
48	8-Oct-05	IRTF 3m	151	13-Nov-05	IRTF 3m
49	2-Aug-03	IRTF 3m	153	10-May-05	IRTF 3m
50	5-Jul-03	IRTF 3m	158	16-Mar-03	IRTF 3m
51	15-Jun-04	IRTF 3m	160	5-Jul-03	IRTF 3m
52	28-Jun-06	IRTF 3m	170	22-Jun-01	IRTF 3m
55	29-Jan-06	IRTF 3m	175	13-Nov-05	IRTF 3m
56	22-Sep-04	IRTF 3m	180	28-Sep-02	IRTF 3m
57	1-Jun-02	IRTF 3m	181	30-Sep-03	IRTF 3m
58	2-Aug-03	IRTF 3m	188	15-Apr-02	IRTF 3m
61	8-Oct-00	IRTF 3m	191	12-Apr-05	IRTF 3m
63	30-Sep-03	IRTF 3m	192	30-Apr-06	IRTF 3m
64	30-Jan-01	IRTF 3m	199	17-Mar-03	IRTF 3m

Object	Obs Date	Telescope	Object	Obs Date	Telescope
201	19-Feb-04	IRTF 3m	596	1-Jun-02	IRTF 3m
205	2-Aug-03	IRTF 3m	599	19-Feb-01	IRTF 3m
210	13-Nov-05	IRTF 3m	606	29-Sep-02	IRTF 3m
221	8-Oct-00	IRTF 3m	625	20-Feb-01	IRTF 3m
236	01-May-06	IRTF 3m	631	29-Sep-02	IRTF 3m
237	15-Apr-02	IRTF 3m	653	17-Mar-03	IRTF 3m
243	17-Mar-03	IRTF 3m	661	16-Mar-03	IRTF 3m
244	29-Mar-01	IRTF 3m	670	29-Sep-02	IRTF 3m
246	9-Mar-05	IRTF 3m	673	21-Jun-01	IRTF 3m
250	16-Oct-03	IRTF 3m	675	15-Apr-02	IRTF 3m
258	24-Aug-01	IRTF 3m	679	19-Feb-01	IRTF 3m
264	19-May-05	IRTF 3m	688	28-Sep-02	IRTF 3m
266	5-Sep-05	IRTF 3m	699	8-Jan-05	IRTF 3m
267	2-Aug-03	IRTF 3m	706	30-Jan-06	IRTF 3m
269	11-May-05	IRTF 3m	716	24-Aug-01	IRTF 3m
278	31-May-02	IRTF 3m	719	23-Aug-01	IRTF 3m
279	8-Jan-05	IRTF 3m	720	9-Oct-00	IRTF 3m
288	29-Sep-02	IRTF 3m	729	14-Aug-01	IRTF 3m
289	29-Jan-01	IRTF 3m	739	28-Sep-02	IRTF 3m
295	28-Sep-02	IRTF 3m	742	16-Mar-03	IRTF 3m
308	18-Apr-05	IRTF 3m	773	22-Sep-04	IRTF 3m
322	29-Sep-02	IRTF 3m	776	12-Apr-05	IRTF 3m
337	28-Sep-02	IRTF 3m	782	22-Jun-01	IRTF 3m
345	8-Oct-05	IRTF 3m	785	11-May-05	IRTF 3m
346	31-May-02	IRTF 3m	789	17-Aug-02	IRTF 3m
349	22-Jun-01	IRTF 3m	793	28-Sep-02	IRTF 3m
352	22-Jun-01	IRTF 3m	808	14-Aug-01	IRTF 3m
354	15-Apr-02	IRTF 3m	824	14-Aug-01	IRTF 3m
359	30-Jan-01	IRTF 3m	832	5-Jul-03	IRTF 3m
371	14-Aug-01	IRTF 3m	832*	3-Mar-05	CFHT 3.6m
378	14-Apr-02	IRTF 3m	847	19-Feb-01	IRTF 3m
387	27-Apr-03	IRTF 3m	863	14-Jan-02	IRTF 3m
389	24-Aug-01	IRTF 3m	908	20-Jul-06	IRTF 3m
402	19-Feb-01	IRTF 3m	913	15-Aug-01	IRTF 3m
403	27-Apr-03	IRTF 3m	925	28-Sep-02	IRTF 3m
433	17-Aug-02	IRTF 3m	944	22-Sep-04	IRTF 3m
434	23-Aug-01	IRTF 3m	944	14-Jun-01	Magellan 6.5m
444	15-Aug-01	IRTF 3m	984	29-Sep-02	IRTF 3m
446	14-Aug-01	IRTF 3m	985	11-May-05	IRTF 3m
453	15-Aug-01	IRTF 3m	1011	12-Jan-02	IRTF 3m
456	17-Jun-02	IRTF 3m	1020	17-Mar-03	IRTF 3m
460	17-Jun-02	IRTF 3m	1036	28-Mar-01	IRTF 3m
485	6-Mar-02	IRTF 3m	1036	26-Jan-04	IRTF 3m
512	16-Oct-04	IRTF 3m	1036	9-Mar-05	IRTF 3m
513	29-Mar-01	IRTF 3m	1036	03-Jun-06	IRTF 3m
532	21-Jun-01	IRTF 3m	1065	8-Mar-05	IRTF 3m
570	20-Feb-04	IRTF 3m	1094	16-Mar-03	IRTF 3m
579	20-Feb-01	IRTF 3m	1126	20-Feb-01	IRTF 3m

*Data from Vernazza et al. (2006)

Object	Obs Date	Telescope	Object	Obs Date	Telescope
1131	19-Feb-04	IRTF 3m	2035	28-Oct-02	IRTF 3m
1131	11-May-05	IRTF 3m	2042	23-Aug01?	IRTF 3m
1139	16-Jun-04	IRTF 3m	2045	14-Jan-02	IRTF 3m
1139	5-Sep-05	IRTF 3m	2063	19-May-05	IRTF 3m
1143	10-Jun-05	IRTF 3m	2064	29-Jun-06	IRTF 3m
1147	15-Aug-01	IRTF 3m	2074	30-Sep-03	IRTF 3m
1148	29-Mar-01	IRTF 3m	2085	14-Apr-02	IRTF 3m
1198	28-Oct-02	IRTF 3m	2099	8-Oct-05	IRTF 3m
1204	19-Feb-04	IRTF 3m	2107	29-Jan-06	IRTF 3m
1228	16-Mar-03	IRTF 3m	2157	16-Mar-03	IRTF 3m
1300	25-Oct-06	IRTF 3m	2246	17-Apr-05	IRTF 3m
1329	17-Aug-02	IRTF 3m	2335	30-Oct-05	IRTF 3m
1332	10-Jun-05	IRTF 3m	2353	31-May-02	IRTF 3m
1350	21-Jun-01	IRTF 3m	2354	17-Mar-03	IRTF 3m
1374	20-Feb-04	IRTF 3m	2378	11-May-05	IRTF 3m
1433	17-Aug-02	IRTF 3m	2386	17-Jun-02	IRTF 3m
1459	20-Feb-01	IRTF 3m	2396	15-Aug-01	IRTF 3m
1471	8-Oct-05	IRTF 3m	2401	17-Aug-02	IRTF 3m
1494	25-Oct-06	IRTF 3m	2442	15-Sep-02	IRTF 3m
1508	19-Feb-04	IRTF 3m	2448	16-Mar-03	IRTF 3m
1542	18-Apr-05	IRTF 3m	2501	12-Jan-02	IRTF 3m
1565	3-Mar-05	IRTF 3m	2504	27-Apr-03	IRTF 3m
1620	29-Jan-01	IRTF 3m	2521	13-Jan-02	IRTF 3m
1640	8-Mar-05	IRTF 3m	2566	16-Sep-02	IRTF 3m
1642	15-Aug-01	IRTF 3m	2579	10-Oct-00	IRTF 3m
1658	30-Jan-01	IRTF 3m	2715	15-Aug-01	IRTF 3m
1659	15-Mar-02	IRTF 3m	2732	15-Aug-01	IRTF 3m
1660	8-Mar-05	IRTF 3m	2851	24-Aug-01	IRTF 3m
1662	17-Mar-03	IRTF 3m	2873	13-Jan-02	IRTF 3m
1667	28-Oct-02	IRTF 3m	2875	16-Mar-02	IRTF 3m
1685	9-Mar-05	IRTF 3m	2911	17-Mar-03	IRTF 3m
1751	22-Jun-01	IRTF 3m	2912	20-Feb-01	IRTF 3m
1807	15-Sep-04	IRTF 3m	2957	16-Mar-03	IRTF 3m
1839	29-Mar-01	IRTF 3m	2965	10-May-05	IRTF 3m
1848	15-Aug-01	IRTF 3m	2977	28-Sep-02	IRTF 3m
1858	14-Apr-02	IRTF 3m	3028	16-Sep-02	IRTF 3m
1862	13-Nov-05	IRTF 3m	3102	9-Oct-00	IRTF 3m
1862	22-Nov-05	IRTF 3m	3103	21-Jun-01	IRTF 3m
1864	29-Mar-01	IRTF 3m	3122	26-Jan-04	IRTF 3m
1866	6-Jan-94	MDM 2.4m	3155	22-Jun-01	IRTF 3m
1866	21-Nov-06	IRTF 3m	3198	10-May-05	IRTF 3m
1903	17-Mar-03	IRTF 3m	3199	3-Mar-05	IRTF 3m
1904	4-Sep-00	IRTF 3m	3200	10-Dec-04	IRTF 3m
1916	14-Aug-01	IRTF 3m	3248	18-Apr-05	IRTF 3m
1929	19-Feb-01	IRTF 3m	3255	16-Sep-02	IRTF 3m
1943	12-Jan-02	IRTF 3m	3317	01-May-06	IRTF 3m
1943	6-Nov-99	Palomar 5m	3363	15-Apr-02	IRTF 3m
1980	25-Oct-06	IRTF 3m	3395	19-Feb-01	IRTF 3m

Object	Obs Date	Telescope	Object	Obs Date	Telescope
3402	30-Sep-03	IRTF 3m	5685	29-Mar-01	IRTF 3m
3402	1-Sep-03	KPNO 4m	5817	22-Sep-04	IRTF 3m
3430	17-Jun-02	IRTF 3m	5840	24-Aug-01	IRTF 3m
3491	17-Jun-02	IRTF 3m	6047	8-Oct-05	IRTF 3m
3511	15-Apr-02	IRTF 3m	6239	26-Jan-04	KPNO 4m
3628	30-Apr-06	IRTF 3m	6386	3-Mar-05	IRTF 3m
3635	12-Nov-05	IRTF 3m	6411	20-Feb-04	KPNO 4m
3701	14-Aug-01	IRTF 3m	6455	28-Oct-02	IRTF 3m
3734	24-Aug-01	IRTF 3m	6585	25-Oct-06	IRTF 3m
3753	8-Oct-05	IRTF 3m	7341	16-Mar-02	IRTF 3m
3788	17-Mar-03	IRTF 3m	7763	1-Jun-02	IRTF 3m
3844	27-Apr-03	IRTF 3m	8334	17-Mar-03	IRTF 3m
3858	20-Feb-04	IRTF 3m	8444	30-Sep-03	IRTF 3m
3873	28-Oct-02	IRTF 3m	17274	10-Oct-00	IRTF 3m
3903	16-Sep-02	IRTF 3m	18736	30-Jan-01	IRTF 3m
3908	15-Sep-04	IRTF 3m	19127	30-Sep-03	IRTF 3m
3910	17-Aug-02	IRTF 3m	19356	30-Jan-01	IRTF 3m
3920	16-Sep-02	IRTF 3m	19356	10-Apr-97	MDM 2.4m
3949	24-Aug-01	IRTF 3m	20786	1-Sep-03	KPNO 4m
4038	28-Oct-02	IRTF 3m	20790	29-Jan-01	IRTF 3m
4055	11-Apr-05	IRTF 3m	22771	16-Oct-03	IRTF 3m
4142	15-Apr-02	IRTF 3m	24475	29-Mar-01	IRTF 3m
4179	15-Sep-04	IRTF 3m	35107	27-Dec-02	IRTF 3m
4188	14-Aug-01	IRTF 3m	36284	16-Mar-02	IRTF 3m
4197	12-Oct-96	MDM 2.4m	53435	25-Oct-06	IRTF 3m
4352	17-Jun-02	IRTF 3m	53435	12-Jan-00	Palomar 5m
4407	24-Aug-01	IRTF 3m	54690	28-Mar-01	IRTF 3m
4417	24-Aug-01	IRTF 3m	54690	17-May-01	KPNO 4m
4451	14-Jan-02	IRTF 3m	66146	1-Sep-03	KPNO 4m
4558	15-Jun-04	IRTF 3m	86450	29-Jan-01	IRTF 3m
4570	21-Jun-01	IRTF 3m	86819	9-Oct-00	IRTF 3m
4688	29-Jan-01	IRTF 3m	89355	16-Mar-02	IRTF 3m
4713	14-Apr-02	IRTF 3m	98943	24-Oct-04	IRTF 3m
4737	17-Jun-02	IRTF 3m	98943	24-Dec-01	Palomar 5m
4995	28-Oct-02	IRTF 3m	137062	27-Oct-02	IRTF 3m
5013	14-Jan-02	IRTF 3m	1989 VA	27-Oct-02	IRTF 3m
5111	5-Sep-05	IRTF 3m	1997 AE12	16-Oct-03	IRTF 3m
5143	25-Oct-06	IRTF 3m	2000 GD2	15-Mar-02	IRTF 3m
5230	5-Sep-05	IRTF 3m	2000 PG3	4-Sep-00	IRTF 3m
5261	11-May-05	IRTF 3m	2000 XL44	29-Jan-01	IRTF 3m
5261	19-May-05	IRTF 3m	2001 MQ3	14-Aug-01	IRTF 3m
5401	16-Mar-03	IRTF 3m	2001 TX16	15-Mar-02	IRTF 3m
5407	13-Jan-02	IRTF 3m	2001 XN254	14-Apr-02	IRTF 3m
5587	28-Mar-01	IRTF 3m	2002 AA	13-Jan-02	IRTF 3m
5604	29-Mar-01	IRTF 3m	2002 AV	13-Jan-02	IRTF 3m
5604	1-Mar-00	KPNO 4m			
5641	12-Apr-05	IRTF 3m			
5660	22-Aug-93	MDM 1.3m			

Appendix C: Principal Component Eigenvectors

Wavelength (microns)	Eigen PC1'	Eigen PC2'	Eigen PC3'	Eigen PC4'	Eigen PC5'
0.45	-0.0766	-0.0643	-0.2724	0.3046	-0.5174
0.50	-0.0391	-0.0279	-0.1270	0.1525	-0.1876
0.60	0.0438	0.0176	0.1128	-0.1486	0.0593
0.65	0.0876	0.0343	0.2104	-0.2677	0.0754
0.70	0.1256	0.0471	0.2726	-0.3386	0.0523
0.75	0.1466	0.0096	0.2475	-0.3284	-0.0231
0.80	0.1271	-0.1186	0.1486	-0.2392	-0.1466
0.85	0.0888	-0.2673	0.0420	-0.1453	-0.2569
0.90	0.0680	-0.3645	-0.0385	-0.0921	-0.2293
0.95	0.0857	-0.3743	-0.1168	-0.0505	-0.0657
1.00	0.1371	-0.2899	-0.2083	-0.0289	0.1077
1.05	0.1921	-0.1527	-0.2809	-0.0277	0.1717
1.10	0.2322	-0.0381	-0.2747	-0.0160	0.1685
1.15	0.2566	0.0306	-0.2169	0.0077	0.1611
1.20	0.2704	0.0708	-0.1713	0.0304	0.1463
1.25	0.2787	0.1053	-0.1427	0.0450	0.1061
1.30	0.2849	0.1385	-0.1031	0.0608	0.0533
1.35	0.2852	0.1598	-0.0407	0.0842	0.0090
1.40	0.2782	0.1645	0.0243	0.1104	-0.0429
1.45	0.2641	0.1520	0.0930	0.1387	-0.0868
1.50	0.2427	0.1192	0.1562	0.1609	-0.1188
1.55	0.2154	0.0689	0.2021	0.1752	-0.1250
1.60	0.1841	0.0089	0.2231	0.1804	-0.1158
1.65	0.1531	-0.0514	0.2215	0.1714	-0.0940
1.70	0.1247	-0.1069	0.2043	0.1550	-0.0757
1.75	0.1002	-0.1532	0.1784	0.1421	-0.0525
1.80	0.0804	-0.1884	0.1508	0.1279	-0.0271
1.85	0.0665	-0.2136	0.1225	0.1095	0.0104
1.90	0.0570	-0.2283	0.0923	0.0868	0.0473
1.95	0.0513	-0.2317	0.0617	0.0610	0.0785
2.00	0.0502	-0.2233	0.0346	0.0358	0.1050
2.05	0.0538	-0.2023	0.0136	0.0103	0.1249
2.10	0.0607	-0.1706	-0.0038	-0.0162	0.1241
2.15	0.0690	-0.1302	-0.0229	-0.0476	0.0916
2.20	0.0778	-0.0852	-0.0447	-0.0838	0.0354
2.25	0.0859	-0.0406	-0.0678	-0.1225	-0.0327
2.30	0.0934	0.0023	-0.0911	-0.1644	-0.1126
2.35	0.0997	0.0438	-0.1153	-0.2068	-0.1993
2.40	0.1050	0.0832	-0.1389	-0.2445	-0.2884
2.45	0.1090	0.1177	-0.1580	-0.2708	-0.3767

Appendix D: Flow chart. It's as easy as 1, 2, 3…

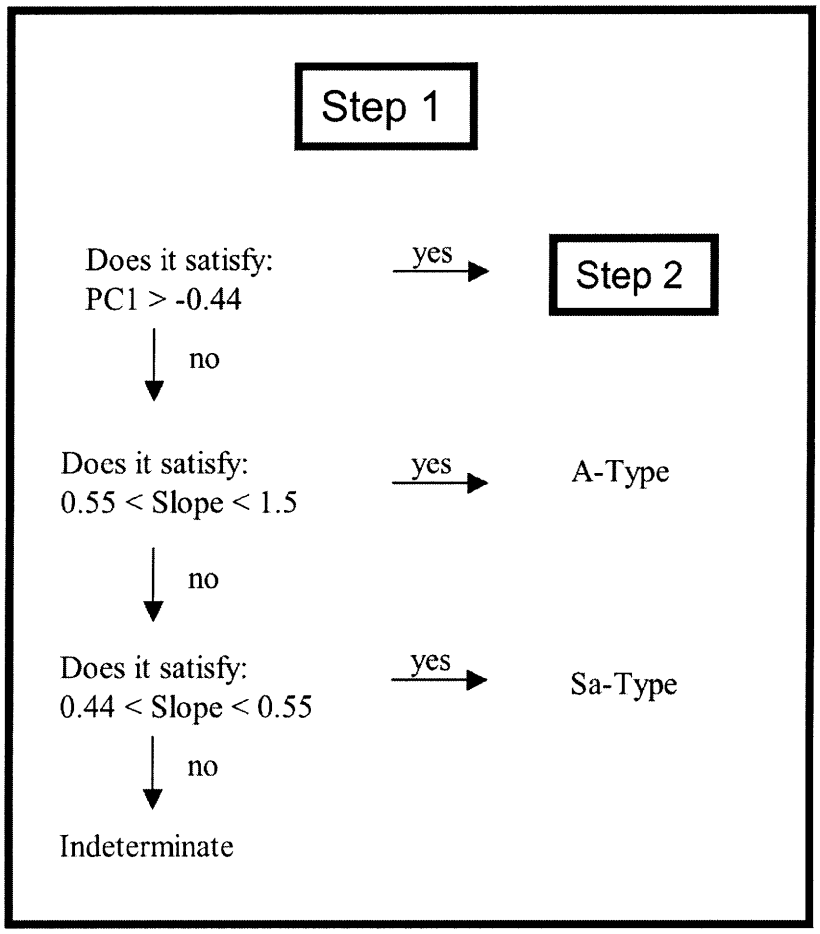

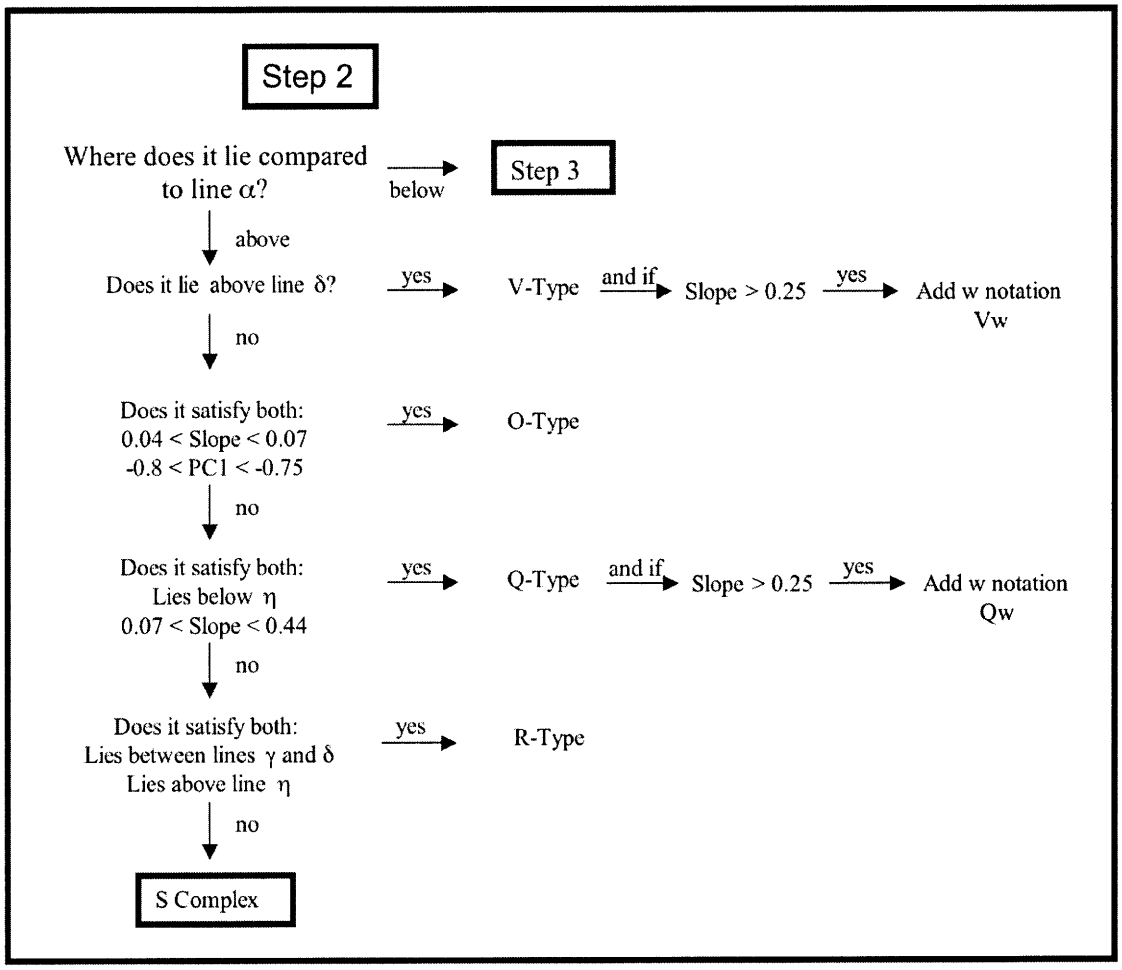
Step 2
Where does it lie compared to line α?
below
Step 3
above
Does it lie above line δ?
yes
V-Type
and if
Slope > 0.25
yes
Add w notation
Vw
no
Does it satisfy both:
0.04 < Slope < 0.07
-0.8 < PC1 < -0.75
yes
O-Type
no
Does it satisfy both:
Lies below η
0.07 < Slope < 0.44
yes
Q-Type
and if
Slope > 0.25
yes
Add w notation
Qw
no
Does it satisfy both:
Lies between lines γ and δ
Lies above line η
yes
R-Type
no
S Complex

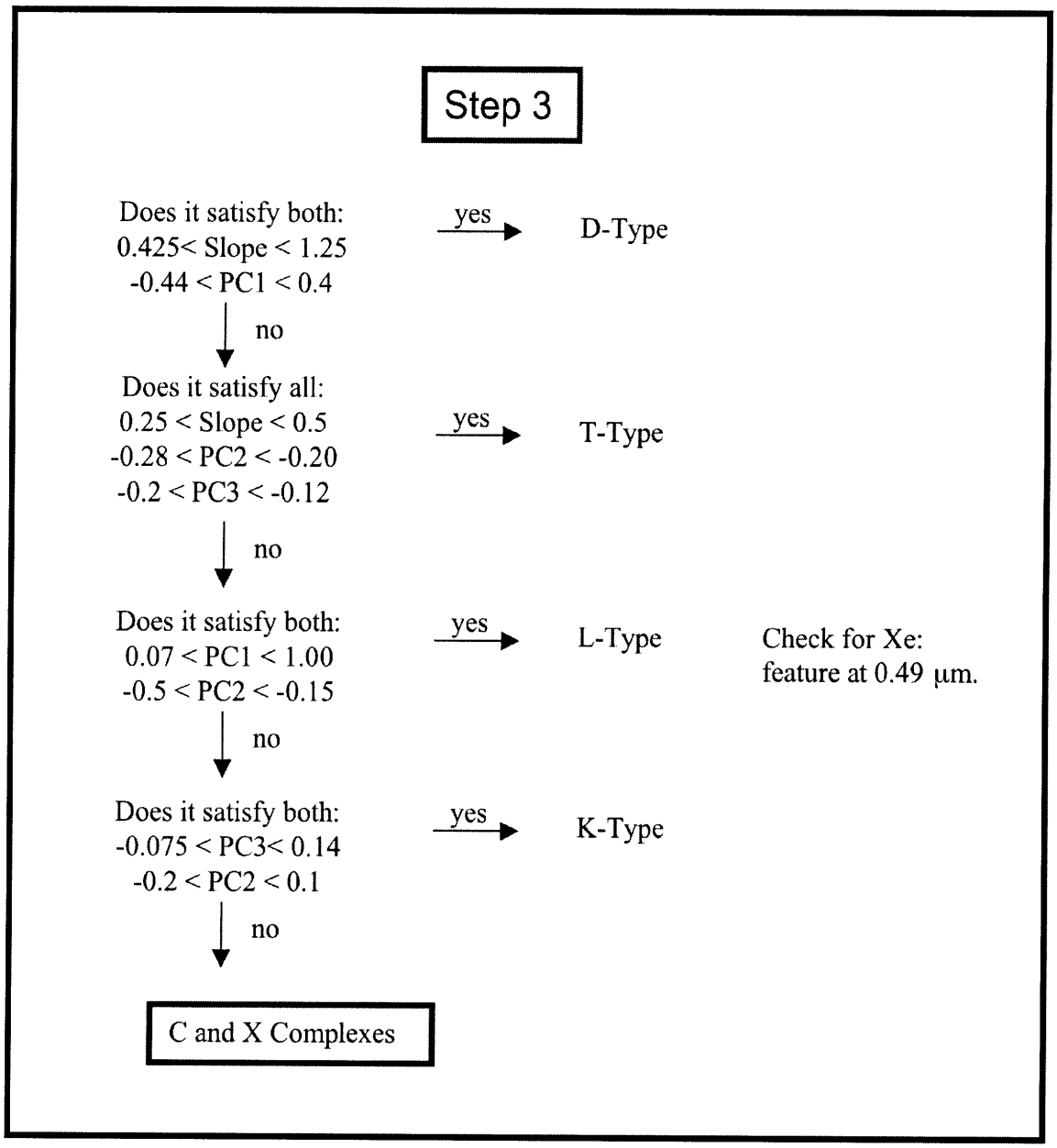
Step 3
Does it satisfy both:
0.425< Slope < 1.25
-0.44 < PC1 < 0.4
yes
D-Type
no
Does it satisfy all:
0.25 < Slope < 0.5
-0.28 < PC2 < -0.20
-0.2 < PC3 < -0.12
yes
T-Type
no
Does it satisfy both:
0.07 < PC1 < 1.00
-0.5 < PC2 < -0.15
yes
L-Type
Check for Xe:
feature at 0.49 μm.
no
Does it satisfy both:
-0.075 < PC3< 0.14
-0.2 < PC2 < 0.1
yes
K-Type
no
C and X Complexes

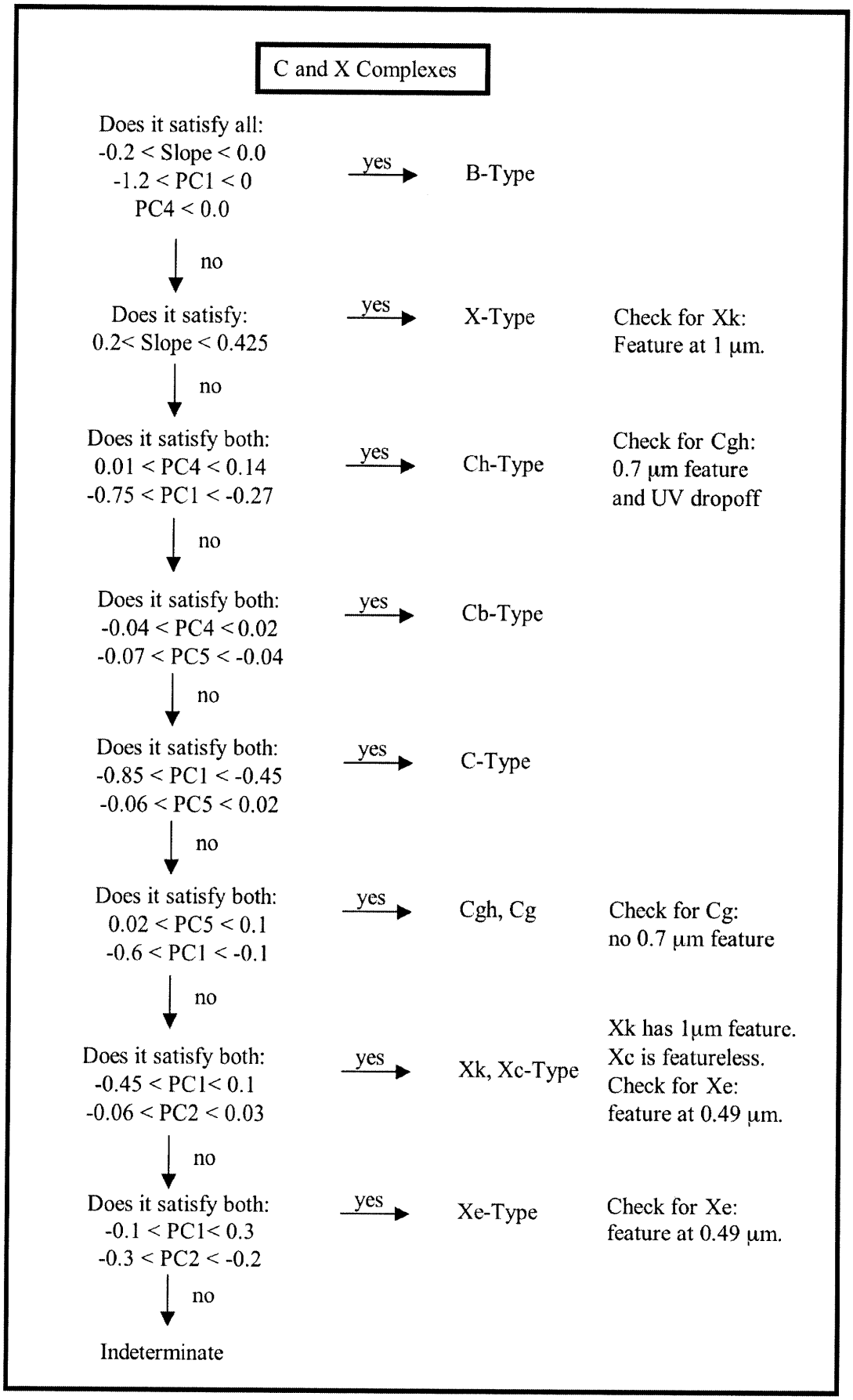
C and X Complexes
Does it satisfy all:
-0.2 < Slope < 0.0
-1.2 < PC1 < 0
PC4 < 0.0
yes
B-Type
no
Does it satisfy:
0.2< Slope < 0.425
yes
X-Type
Check for Xk:
Feature at 1 μm.
no
Does it satisfy both:
0.01 < PC4 < 0.14
-0.75 < PC1 < -0.27
yes
Ch-Type
Check for Cgh:
0.7 μm feature
and UV dropoff
no
Does it satisfy both:
-0.04 < PC4 < 0.02
-0.07 < PC5 < -0.04
yes
Cb-Type
no
Does it satisfy both:
-0.85 < PC1 < -0.45
-0.06 < PC5 < 0.02
yes
C-Type
no
Does it satisfy both:
0.02 < PC5 < 0.1
-0.6 < PC1 < -0.1
yes
Cgh, Cg
Check for Cg:
no 0.7 μm feature
no
Does it satisfy both:
-0.45 < PC1< 0.1
-0.06 < PC2 < 0.03
yes
Xk, Xc-Type
Xk has 1μm feature.
Xc is featureless.
Check for Xe:
feature at 0.49 μm.
no
Does it satisfy both:
-0.1 < PC1< 0.3
-0.3 < PC2 < -0.2
yes
Xe-Type
Check for Xe:
feature at 0.49 μm.
no
Indeterminate

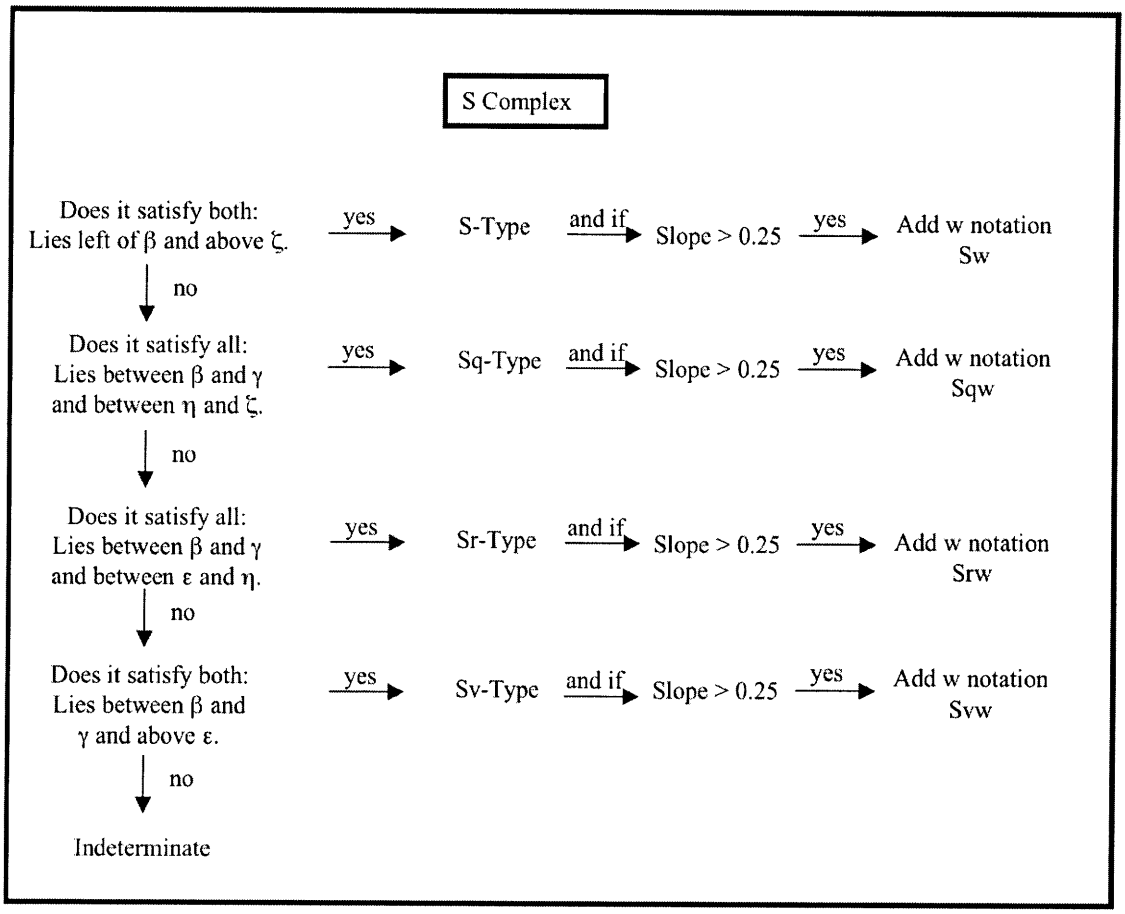

Checks* for Cg, Cgh, Xc, Xe, Xk

Cg: Strong UV absorption feature before 0.55 μm

Cgh: A Cg with a broad, shallow absorption feature at 0.7 μm.

Xc: Red and featureless with slight concave-down curvature.

Xe: Concave-up absorption feature before 0.55 μm.

Xk: Red with a flat section around 0.75 μm.

*These spectral features all exist in the visible and were identified in the Bus system (Bus 1999)

Equations

PC1' = -3PC2' - 0.28	Line α
PC1' = -3PC2' + 0.35	Line β
PC1' = -3PC2' + 1.00	Line γ
PC1' = -3PC2' + 1.50	Line δ
PC1' = 1/3PC2' + 0.55	Line ε
PC1' = 1/3PC2' - 0.10	Line ζ
PC1' = 1/3PC2' - 0.40	Line η

Appendix E: New Labels to Data

Object	Bus Class	DeMeo Class	Slope	PC1'	PC2'	PC3'	PC4'	PC5'
1	C	C	0.0060	-0.5626	-0.0669	-0.1351	-0.0871	-0.0256
2	B	B	-0.0892	-0.5691	-0.0640	-0.1550	-0.0916	-0.0458
3	Sk	Sq	0.1775	-0.1930	0.0610	-0.0033	0.0218	0.0038
4	V	V	0.0270	-0.0043	0.6020	-0.1556	0.0189	-0.0255
5	S	S	0.1074	0.1467	-0.0250	-0.0161	-0.0212	0.0158
7	S	Sq	0.1930	-0.1141	-0.0240	0.0654	-0.0415	-0.0042
8		Sw	0.2902	0.2597	-0.1399	0.1139	-0.0320	-0.0538
10	C	C	0.1391	-0.7550	0.0246	-0.1519	-0.0311	-0.0107
11	Sk	Sq	0.2127	-0.3055	0.0236	-0.0003	-0.0168	-0.0016
13	Ch	Ch	0.0757	-0.4139	-0.0506	-0.1363	0.0849	0.0080
14	S	S	0.1706	0.0743	-0.0488	-0.0363	0.0153	0.0095
15	S	Sq	0.1581	-0.1553	-0.0189	0.0614	-0.0094	-0.0116
16	X	X	0.2810	-0.0253	-0.1749	-0.1528	0.0054	-0.0013
17	Sl	S	0.2103	0.4067	-0.1167	-0.0095	0.0088	0.0096
18	S	S	0.1636	0.2243	-0.1079	-0.0199	-0.0013	0.0195
19	Ch	Ch	0.1935	-0.5654	-0.0102	-0.1606	0.0874	0.0176
20	S	S	0.0811	0.0203	0.0044	-0.0221	-0.0411	0.0071
21	Xk	Xk	0.0678	-0.0574	-0.1942	-0.1419	0.0333	-0.0317
22	X	X	0.3008	-0.3406	-0.1302	-0.1396	-0.0003	0.0118
24	B	C	0.0552	-0.8310	0.0332	-0.2165	-0.0956	-0.0358
25	S	S	0.2062	0.1640	-0.0107	0.1429	0.0144	-0.0279
26	S	S	0.1836	-0.0214	0.0007	0.1135	0.0176	0.0070
27	S	S	0.2268	0.0712	-0.0064	0.1212	0.0233	-0.0026
28	S	S	0.1378	0.2968	-0.0959	0.0218	-0.0149	0.0090
29	S	S	0.2008	0.1264	-0.1190	-0.0160	0.0138	0.0041
30	Sl	S	0.2165	0.3434	-0.1621	0.0467	-0.0064	-0.0149
32	S	Sw	0.2623	0.0878	0.0323	-0.0068	0.0417	0.0330
33	Sq	S	0.0996	0.0297	0.0872	-0.0577	0.0551	0.0353
34	Ch	Ch	0.0717	-0.3325	-0.0385	-0.1890	0.0935	0.0007
37	S	S	0.1782	0.2766	-0.0926	0.0083	-0.0177	0.0127
38	Cgh	Cgh	0.1219	-0.2905	-0.0760	-0.1458	0.0687	0.0450
39	S	Sqw	0.2720	-0.1372	-0.0209	0.1027	0.0434	-0.0457
40	S	S	0.1209	0.0628	-0.0945	0.0195	-0.0615	-0.0012
41	Ch	Sq	0.1834	-0.3458	0.0588	-0.1160	0.1253	-0.0192
42	L	K	0.2132	-0.0639	-0.1695	0.1133	-0.0471	-0.0477
43	Sk	Sq	0.1972	-0.1731	0.0816	0.0944	0.0660	-0.0134
48	Ch	Ch	0.0207	-0.6803	0.0187	-0.1861	0.0556	0.0005
49	Ch	Ch	0.0078	-0.4755	-0.0095	-0.1750	0.0830	0.0203
50	Ch	Ch	0.0460	-0.5934	0.0395	-0.2039	0.0927	0.0079
51	Ch	Ch	0.1844	-0.3110	-0.0788	-0.0922	0.1159	0.0468
52	C	C	0.1779	-0.6801	-0.0223	-0.1447	-0.1142	0.0066
55	X	X	0.2668	-0.3587	-0.0564	-0.1573	0.0262	-0.0015
56	Xk	Xk	0.1499	-0.1423	-0.1582	-0.1015	-0.0569	0.0014
57	S	S	0.1680	0.2697	-0.0700	-0.0333	0.0198	0.0065
58	Ch	Ch	0.0167	-0.4620	-0.0242	-0.1881	0.0638	0.0108
61	S	S	0.1664	0.3411	-0.0905	-0.0071	-0.0124	0.0126
63	Sa	S	0.2382	0.3774	-0.1165	0.1057	-0.0713	-0.0184
64	Xe	Xe	0.1201	0.0463	-0.2407	-0.0967	-0.0392	-0.0059

Object	Bus Class	DeMeo Class	Slope	PC1'	PC2'	PC3'	PC4'	PC5'
65	Xc	Xk	0.1823	-0.4111	-0.0376	-0.1855	-0.0464	-0.0115
66	Ch	Ch	0.1009	-0.4739	-0.0377	-0.1799	0.0362	0.0071
67	S	S	0.1534	0.1438	0.0272	0.0028	-0.0178	0.0214
69	X	X	0.2946	-0.3394	-0.0517	-0.1497	0.0216	0.0060
70	Ch	Ch	0.1214	-0.2771	-0.0617	-0.1589	0.1165	0.0309
73		S	0.2182	0.4242	-0.0500	-0.0310	0.0453	0.0243
76	X	X	0.2479	-0.6309	-0.0148	-0.1679	-0.0355	-0.0054
77	Xe	Xe	0.1781	-0.0892	-0.2235	-0.1153	-0.0244	-0.0141
78	Ch	Ch	0.1192	-0.5045	-0.0302	-0.1790	0.0372	0.0241
82	Sq	S	0.0514	0.0305	0.0415	-0.0687	0.0479	-0.0166
84	Ch	Ch	0.0764	-0.4183	-0.0480	-0.1660	0.0696	-0.0023
85	B	C	0.1047	-0.7800	0.0348	-0.1901	-0.0317	-0.0360
87	X	X	0.2873	-0.3383	-0.0866	-0.1944	-0.0119	-0.0171
90	C	C	0.1902	-0.7534	0.0431	-0.1747	-0.0556	-0.0195
92	Xc	Xk	0.1604	-0.2105	-0.0825	-0.1616	0.0231	-0.0113
93	C	C	0.0235	-0.5609	-0.0721	-0.1823	-0.1202	-0.0490
96	T	T	0.2672	0.0024	-0.2296	-0.1353	0.0032	-0.0221
97	X	Xc	0.0782	-0.1431	-0.2083	-0.1168	-0.0371	0.0035
99	Xk	Xk	0.0906	-0.0986	-0.1395	-0.1146	0.0174	0.0149
101	S	S	0.1685	0.1674	-0.0220	0.0347	-0.0371	0.0377
103	S	S	0.1399	0.1377	-0.0870	0.0598	-0.0932	-0.0041
105	Ch	Ch	0.0901	-0.3221	-0.0785	-0.1738	0.0629	-0.0017
106	Cgh	Cgh	0.0460	-0.5045	0.0048	-0.1215	0.0594	0.0584
108	Sl	Sw	0.2713	0.2950	-0.0596	0.0671	-0.0020	0.0111
110	X	X	0.2413	-0.2178	-0.0643	-0.1567	0.0837	0.0076
111	Ch	Ch	-0.0038	-0.3827	-0.0731	-0.1973	0.0372	-0.0125
114	Xk	K	0.2282	-0.2364	-0.1662	-0.0634	-0.0363	-0.0261
115	S	S	0.1408	0.3346	-0.0679	0.0258	-0.0233	0.0095
119	Sl	S	0.2329	0.2297	-0.0735	0.1495	-0.0176	-0.0105
128	C	C	0.0909	-0.4973	-0.0827	-0.1416	-0.0643	-0.0133
130	Ch	Ch	0.0925	-0.5175	0.0020	-0.1308	0.0706	0.0491
131	Xc	K	0.1741	-0.5109	0.0313	-0.0507	-0.0184	0.0174
132	Xe	Xe	0.1041	-0.3640	-0.0944	-0.1157	-0.0160	0.0129
133	S	S	0.1715	0.1898	-0.0812	0.1374	-0.0473	-0.0146
147	C	C	0.1778	-0.6347	-0.0061	-0.1881	-0.0282	-0.0113
150	Cb	C	0.1558	-0.6658	-0.0221	-0.1946	-0.0545	-0.0296
151	Sl	Sw	0.3780	0.3427	-0.1232	0.1094	0.0687	0.0251
153	X	X	0.2534	-0.4440	-0.0551	-0.1702	0.0172	-0.0073
158	S	S	0.2067	-0.0603	0.0573	0.0102	0.0080	0.0349
160	C	Ch	0.1421	-0.3880	-0.0567	-0.1572	0.0260	0.0052
170	S	S	0.1472	0.2552	-0.0862	0.0138	-0.0673	0.0208
175	Cg	Cg	0.1176	-0.5537	-0.0130	-0.1130	-0.0558	0.0288
180	Sq	Sr	0.1161	0.1465	0.0934	-0.0583	0.0595	0.0310
181	Xk	Xk	0.0317	-0.0403	-0.1862	-0.0815	-0.0389	-0.0390
188	S	S	0.1690	0.3672	-0.0820	0.0267	0.0087	0.0322
191	Cb	Cb	0.1738	-0.5579	-0.0200	-0.1974	-0.0077	-0.0406
192	Sl	Sw	0.3086	0.2612	-0.0848	0.1100	0.0020	-0.0166
199	X	X	0.4045	-0.1176	-0.1249	-0.1555	0.0677	-0.0176

Object	Bus Class	DeMeo Class	Slope	PC1'	PC2'	PC3'	PC4'	PC5'
201	X	X	0.2004	-0.2912	-0.0816	-0.1636	0.0088	-0.0039
205	Ch	Ch	0.0580	-0.3641	-0.0512	-0.1768	0.0775	0.0034
210	Cb	Cb	0.0904	-0.6191	-0.0086	-0.1561	-0.0225	-0.0535
221	K	K	0.0158	-0.2598	-0.1234	-0.0137	-0.1170	-0.0340
236	L	L	0.2144	0.2180	-0.2586	-0.0019	-0.0215	-0.0179
237	S	Sr	0.1800	0.3735	0.0136	-0.0128	0.0081	0.0446
243	S	S	0.2191	0.0410	0.0275	-0.0348	0.0044	0.0330
244	Sa	Sw	0.3561	0.3378	-0.1351	0.0436	0.0821	-0.0523
246	A	A	0.6036	-0.5975	-0.0238	0.4431	-0.1020	-0.0245
250	Xk	Xk	0.2586	-0.1308	-0.0905	-0.1378	0.0100	0.0049
258	S	S	0.1388	0.2412	0.0206	0.0163	-0.0058	0.0309
264	S	S	0.2022	0.1715	-0.0041	-0.0186	0.0359	0.0132
266	Ch	Ch	0.0988	-0.5608	0.0061	-0.1624	0.0658	0.0138
267	D	D	0.4505	0.2669	-0.2875	-0.1235	0.0750	-0.0073
269	Ld	D	1.2478	0.1062	-0.2237	-0.1521	0.0427	0.0112
278	S	S	0.2441	0.1226	0.0262	0.0702	0.0545	-0.0071
279	X	D	0.5886	-0.4233	-0.0246	-0.1842	0.1432	-0.0294
288	S	S	0.1642	0.4438	-0.1252	0.0143	-0.0161	0.0303
289	A	A	1.3827	-1.6620	0.3082	0.5455	0.0231	0.0879
295	S	Sw	0.2925	0.0453	-0.0111	0.1110	0.0651	-0.0231
308	T	T	0.3187	0.0562	-0.2577	-0.1384	-0.0282	-0.0111
322	X	X	0.4013	-0.3421	-0.0455	-0.1527	0.0614	-0.0023
337	X	Xk	0.1473	-0.3521	-0.0320	-0.1549	0.0096	-0.0020
345	Ch	Ch	0.1286	-0.7064	0.0298	-0.1702	0.0548	0.0009
346	S	S	0.1786	-0.0587	0.0521	0.0566	0.0262	-0.0022
349	R	R	0.3213	-0.2178	0.4352	0.1189	-0.0615	-0.0050
352	Sl	Sw	0.2949	-0.0003	-0.0087	0.1840	-0.0119	-0.0125
354	Sl	A	0.7342	-0.4539	0.0124	0.2931	0.0412	-0.0253
359	X	Xk	0.1163	-0.2590	-0.0821	-0.1642	0.0400	-0.0346
371	S	S	0.1721	0.3812	-0.0676	0.0057	0.0058	0.0286
378	S	S	0.1637	0.3610	-0.1108	-0.0042	0.0046	0.0304
387	L	L	0.1144	0.5320	-0.3402	-0.0064	-0.0426	-0.0539
389	S	S	0.1184	0.0829	-0.0296	-0.0267	0.0057	0.0146
402	K	L	0.0471	0.1322	-0.2091	-0.0456	0.0060	-0.0371
403	S	S	0.1814	-0.0047	-0.0166	0.0836	0.0227	-0.0060
433	S	Sw	0.2762	0.0787	-0.0135	0.1850	-0.0179	-0.0148
434	Xe	Xe	0.0919	0.0091	-0.2038	-0.0462	-0.0941	0.0350
444	C	C	0.1228	-0.6121	0.0062	-0.1916	-0.0750	-0.0043
446	A	A	0.7809	-0.7220	0.0743	0.6009	0.0145	-0.0383
453	S	Sw	0.2547	-0.0338	-0.0309	0.1606	-0.0368	0.0078
456	S	S	0.2361	0.1184	-0.0210	0.1282	0.0166	-0.0141
460	K	L	-0.0050	0.4365	-0.2682	-0.0788	0.0035	-0.0065
485	S	S	0.1651	0.1581	0.0148	0.0029	0.0520	0.0026
512	S	Sqw	0.2918	-0.1499	0.0803	0.2015	0.0160	0.0016
513	K	K	0.0157	-0.0649	-0.1890	0.0288	-0.1564	-0.0340
532	S	S	0.1781	0.0197	-0.0408	0.0319	-0.0135	-0.0177
570	T	T	0.4169	0.1411	-0.2291	-0.1314	0.0819	0.0329
579	K	K	0.1296	-0.1851	-0.1318	-0.0009	-0.0100	-0.0241

Object	Bus Class	DeMeo Class	Slope	PC1'	PC2'	PC3'	PC4'	PC5'
596	T	T	0.2836	0.0374	-0.2216	-0.1808	0.0021	-0.0279
599	K	L	0.1751	0.1626	-0.1783	-0.0262	0.0394	-0.0041
606	K	L	0.1701	0.2644	-0.2600	-0.0666	0.0145	0.0114
625	Sa	Sw	0.4198	0.4090	-0.1305	0.2046	0.0687	-0.0098
631	S	S	0.1695	0.1668	-0.0136	0.0322	-0.0242	0.0373
653	K	K	0.1222	-0.1679	-0.1498	-0.0035	-0.0703	-0.0072
661	K	K	0.0910	-0.0712	-0.1698	-0.0149	-0.0415	-0.0367
670	S	S	0.0748	0.2028	0.0193	-0.0003	0.0244	0.0141
673	S	L	0.1012	0.4082	-0.3053	-0.0949	-0.0627	0.0020
675	S	Sw	0.2698	-0.0684	-0.0132	0.0450	0.0218	0.0048
679	K	L	0.1343	0.2956	-0.2743	-0.0309	0.0426	0.0108
688	C	C	0.1442	-0.5997	-0.0120	-0.1869	-0.0725	-0.0107
699	Sq	S	0.1172	-0.0720	0.0366	0.0116	0.0467	0.0081
706	Cgh	Cgh	0.1744	-0.5633	0.0475	-0.0812	0.2141	0.0726
716	S	S	0.0861	0.4545	-0.1267	-0.0224	-0.0032	0.0232
719		S	0.1976	0.1490	-0.0287	0.0772	0.0078	-0.0304
720	Sq	Sq	0.0856	-0.1298	0.0391	-0.0386	0.0036	0.0346
729	L	L	0.2592	0.2035	-0.2531	0.0273	-0.0633	0.0190
739	X	Xc	0.1825	-0.2526	-0.1227	-0.1680	-0.0181	0.0019
742	K	K	0.1083	-0.2484	-0.1032	-0.0032	-0.0390	-0.0113
773	T	T	0.3027	0.1142	-0.2490	-0.1274	0.0177	0.0032
776	Cgh	Cgh	0.1045	-0.1868	-0.1188	-0.1460	0.0264	0.0473
782	Sl	Sw	0.3368	0.0608	-0.0072	0.1467	0.0671	-0.0250
785	Cb	Cb	0.1886	-0.5012	-0.0460	-0.2471	0.0059	-0.0661
789	X	X	0.2191	-0.3208	-0.0605	-0.1676	0.0007	0.0072
793	S	S	0.1374	0.2352	-0.0073	-0.0096	-0.0123	0.0300
808	Sq	Sr	0.1693	0.0862	0.0915	-0.0014	0.0518	0.0239
824	L	L	0.0120	0.4266	-0.3690	-0.0526	-0.1061	-0.0267
832		S	0.1270	0.0897	-0.0428	-0.0827	0.0706	-0.0251
847	S	S	0.2065	0.1657	0.0385	0.0531	0.0338	0.0618
863	A	A	0.8746	-0.7688	0.1836	0.5417	0.0295	-0.0590
908	L	D	0.6858	-0.0216	-0.1444	-0.0045	0.2364	0.0957
913	Sa	Sw	0.3593	0.2196	-0.0639	0.1825	0.0032	-0.0164
925	S	S	0.1022	0.3738	-0.0883	-0.0133	0.0133	0.0088
929	S	S	0.2074	0.1117	-0.0501	0.1472	-0.0539	-0.0012
944		D	0.6300	0.2156	-0.3083	-0.1251	-0.0059	0.0008
984	Sr	Sa	0.4377	-0.6705	0.1555	0.4003	-0.0513	-0.0021
985	S	S	0.1807	-0.0410	0.0211	0.1118	-0.0973	-0.0536
1011	Sr	Sw	0.2929	-0.0775	0.0579	0.2634	-0.0301	0.0263
1020	S	Sr	0.1983	0.2683	0.0304	0.0328	0.0114	0.0402
1036	S	Sr	0.1217	0.3906	-0.0041	-0.0157	0.0087	0.0310
1065	S	S	0.2303	0.0672	-0.0003	0.1669	-0.0086	-0.0101
1094	Xk	Xk	0.2185	0.0318	-0.1897	-0.0990	0.0497	-0.0212
1126	A	Sw	0.3941	0.2410	-0.0503	0.2384	0.0130	0.0301
1131	S	S	0.1480	0.1474	-0.0673	0.1983	-0.0362	-0.0050
1139	S	Sw	0.3114	-0.0401	0.0462	0.2062	0.0016	-0.0152
1143		D	0.7547	0.0654	-0.2636	-0.0978	0.1332	-0.0107
1147	S	Sw	0.2828	0.0410	-0.0232	0.1653	-0.0255	0.0267

Object	Bus Class	DeMeo Class	Slope	PC1'	PC2'	PC3'	PC4'	PC5'
1148	K	K	0.1189	-0.2024	-0.1099	0.0499	-0.0615	0.0004
1198		Sw	0.3904	0.3122	-0.1438	-0.0191	0.0827	-0.0193
1204	S	Sw	0.2876	-0.0614	0.0101	0.1076	0.0413	-0.0186
1228	S	Sr	0.2048	0.2914	0.0708	0.0311	0.0319	0.0398
1300	Cg	Cg	0.1054	-0.2599	-0.0818	-0.0837	0.0223	0.0834
1329	S	Sqw	0.3086	-0.1273	0.0168	0.1732	-0.0082	0.0150
1332	Ld	L	0.1529	0.0813	-0.3061	-0.1331	-0.3096	-0.0867
1350	Sa	S	0.2257	0.3398	-0.1171	0.0641	-0.1238	0.0803
1374	Sq	Sq	0.1482	-0.3566	0.1170	0.1614	0.0002	0.0058
1433	S	S	0.1563	-0.0107	0.0712	0.0725	0.0117	0.0271
1459		Vw	0.3246	0.3316	1.3060	-0.2959	-0.2269	-0.1211
1471	T	D	0.7780	-0.3535	-0.0673	-0.1656	0.0479	0.0060
1494	Sa	Sqw	0.3476	-0.1320	0.0756	0.2302	-0.0403	0.0252
1508	C	B	-0.0249	-0.4553	-0.0766	-0.1418	-0.0690	-0.0088
1542	D	D	0.7210	0.1271	-0.1903	-0.1536	0.1144	0.0121
1565	Sq	S	0.0735	-0.0435	0.0890	-0.1931	-0.1628	0.1260
1620	S	S	0.1637	-0.0288	0.0273	0.1421	0.0505	-0.0231
1640	S	S	0.1595	0.0811	-0.0334	0.0752	0.0067	-0.0353
1642	S	S	0.0905	0.4415	-0.0859	0.0300	-0.0789	0.0501
1658		S	0.2413	0.5240	-0.1647	0.0594	0.0760	-0.1031
1659	S	S	0.1635	0.3504	-0.0797	-0.0459	0.0492	-0.0312
1660	S	S	0.1779	0.2259	-0.0131	0.0062	0.0255	0.0337
1662	Sr	Sr	0.1815	0.4950	-0.0014	0.0852	-0.0094	0.0610
1667	Sa	Sw	0.3046	0.2717	-0.0619	0.2316	0.0180	0.0174
1685	S	S	0.0941	-0.0566	0.0256	0.1330	-0.0230	-0.0037
1751	S	S	0.1143	0.3150	-0.1147	0.0020	-0.0945	-0.0117
1807	S	Sqw	0.3380	-0.2285	0.1384	0.0738	0.0275	-0.0119
1839	S	S	0.0519	0.1526	0.0026	0.0323	-0.1107	-0.0174
1848	S	S	0.1435	0.2404	-0.0564	0.0716	-0.1098	0.0726
1858	L	S	0.1504	0.5822	-0.2625	0.0029	0.0101	0.0387
1862	Q	Q	0.1132	-0.4924	0.1862	0.2229	-0.0743	-0.0133
1864	Sr	Sq	0.0528	-0.2706	0.1082	0.1794	-0.0888	0.0619
1866	S	Sw	0.3453	0.0700	-0.0057	0.0700	-0.0052	0.0510
1903	K	K	0.1249	-0.0241	-0.1681	-0.0055	-0.0425	-0.0199
1904	R	V	0.1483	0.2755	0.5257	-0.0271	-0.0874	-0.0654
1916		Sw	0.3902	-0.0124	0.0565	0.0945	0.0145	-0.0035
1929	V	V	0.2193	1.0772	0.9150	-0.0068	0.0364	-0.0233
1943		Sw	0.2732	0.1740	-0.0746	0.0776	0.0524	0.0061
1980	Sl	Sw	0.4071	-0.0144	0.0523	0.1891	0.0235	0.0373
2035	Xe	Xe	0.0876	0.1472	-0.2595	-0.0942	-0.0104	0.0300
2042	Sq	Sr	0.0800	0.1890	0.0736	-0.0102	-0.0016	0.0046
2045	V	V	0.1814	0.7055	0.8418	-0.0965	0.0756	-0.0684
2063	Sq	Sq	0.0700	-0.3144	0.0660	0.1375	-0.0653	0.0226
2064	S	Sqw	0.2569	-0.1839	0.0195	0.1767	0.0041	0.0066
2074		Sq	0.4562	0.1019	0.0440	0.1746	0.0269	-0.0534
2085	L	L	0.0454	0.4460	-0.3548	-0.0183	-0.0488	-0.0129
2099	Ch	Ch	0.1207	-0.5875	0.0166	-0.1875	0.0193	-0.0002
2107	S	S	0.2481	0.0580	-0.0705	0.0931	-0.0806	0.0095

Object	Bus Class	DeMeo Class	Slope	PC1'	PC2'	PC3'	PC4'	PC5'
2157	S	S	0.1897	0.1990	-0.0655	0.0722	-0.0001	0.0245
2246	D	D	0.5312	0.2511	-0.2110	-0.1341	0.1233	0.0023
2335		S	0.2315	0.2507	-0.0416	0.0520	-0.0771	0.0458
2353	S	S	0.0935	0.3713	-0.0718	-0.0252	0.0137	0.0303
2354	L	L	0.0775	0.6610	-0.3559	0.0723	-0.0512	0.0024
2378	Cgh	Cgh	0.0583	-0.5495	0.0086	-0.1693	-0.0034	0.0288
2386	S	S	0.1774	0.2766	-0.0508	0.0422	0.0113	0.0136
2396	Sa	S	0.1849	0.2953	-0.1191	0.1750	-0.0343	0.0169
2401	S	S	0.1744	0.2766	0.0200	-0.0249	-0.0367	-0.0399
2442		V	0.1571	0.8876	0.9743	-0.2123	-0.0100	-0.0243
2448	L	L	0.3125	0.4253	-0.3012	-0.0427	0.0606	0.0336
2501	A	A	0.8437	-0.6265	0.0916	0.6472	0.1271	-0.0803
2504	Sq	Sr	0.1126	0.0951	0.0954	-0.0293	0.0582	0.0279
2521	S	S	0.0789	0.0866	-0.0090	0.0278	-0.0296	-0.0044
2566	V	V	0.0441	0.7136	0.8479	-0.1093	0.0515	-0.0638
2579	V	V	0.0889	0.3419	0.8659	0.2123	0.0075	-0.1497
2715	A	Sw	0.3118	0.3235	-0.1613	0.2232	-0.0447	-0.0086
2732	A	L	0.2002	0.7163	-0.3427	0.1762	-0.1555	0.0295
2851	V	V	0.1538	0.6727	0.9608	-0.1887	-0.2213	0.0734
2873	Sq	Sq	0.1345	-0.1752	0.1131	0.1473	0.0673	-0.0298
2875	S	S	0.1293	0.2965	-0.0846	0.0667	-0.0463	0.0142
2911	S	Sw	0.2679	0.2209	-0.0071	0.0910	0.0362	0.0121
2912	V	V	0.1982	0.6001	1.1117	-0.2085	-0.0381	0.0291
2957	K	K	0.1449	0.0173	-0.1566	-0.0374	-0.0121	-0.0254
2965		Sv	0.1904	0.6981	0.0147	-0.0233	0.0985	0.0146
2977	S	S	0.1668	0.2776	-0.0690	0.0350	-0.0031	0.0122
3028	K	K	0.0103	-0.1513	-0.1396	-0.0696	-0.1012	-0.0266
3102		Sqw	0.2604	-0.2280	0.0881	0.1889	-0.0515	-0.0098
3103	Xe	Xe	0.1303	0.2177	-0.2795	-0.0829	-0.0694	0.0452
3122	S	Qw	0.3829	-0.3772	0.1962	0.2076	0.0580	-0.0115
3155	V	V	0.0533	1.1248	0.8416	-0.3899	-0.1176	0.1033
3198	S	Sqw	0.3354	-0.1666	0.0490	0.2175	0.1583	-0.0899
3199	Sq	K	0.2273	-0.6353	0.0481	0.1171	0.0337	0.0088
3200	B	B	-0.1626	-1.0224	0.1534	-0.2026	-0.1287	-0.0123
3248	D	D	0.4834	0.3439	-0.2783	-0.1477	0.0552	0.0161
3255	S	S	0.0995	0.1948	0.0432	0.0164	0.0118	0.0365
3317	T	D	0.5051	-0.0303	-0.1559	-0.1150	0.1130	-0.0036
3363	Sq	Sr	0.1822	-0.1342	0.1633	0.0017	0.0243	0.0420
3395	Sr	S	0.1660	0.1479	0.0625	0.0421	0.0495	0.0724
3402		S	0.2381	0.2431	-0.0662	0.1002	-0.0218	-0.0368
3430	Sq	S	0.0860	0.2024	0.0258	-0.0155	0.0458	0.0283
3491	Sq	S	0.0196	0.1475	0.0507	-0.0419	-0.0231	0.0199
3511	S	Srw	0.3246	0.0134	0.1181	0.0887	0.0018	0.0191
3628	O	O	0.0572	-0.7900	0.5696	0.3075	0.1764	-0.1059
3635	S	Srw	0.2767	0.1795	0.1094	0.0258	0.0407	0.0055
3701	S	S	0.1225	0.2605	-0.0192	-0.0132	-0.0652	0.0051
3734	Ld	L	0.0807	0.7779	-0.4665	0.0210	-0.0144	-0.0224
3753	Q	Q	0.2115	-0.5643	0.2866	0.0835	0.0046	-0.0157

Object	Bus Class	DeMeo Class	Slope	PC1'	PC2'	PC3'	PC4'	PC5'
3788	S	S	0.2012	0.2111	-0.0168	0.0719	0.0036	-0.0033
3844	L	L	0.0026	0.6056	-0.3788	-0.0330	-0.0933	-0.0427
3858	Sa	Srw	0.2680	-0.0163	0.1400	0.3209	-0.1941	0.1521
3873	S	Sw	0.2665	0.0244	0.0483	0.0577	0.0638	-0.0090
3903	Sq	S	0.0416	-0.0145	0.0422	-0.0252	-0.0171	0.0191
3908		V	-0.0188	0.5903	1.3071	-0.3046	0.0383	0.0846
3910	S	S	0.2282	0.1284	-0.0008	0.0866	-0.0237	0.0239
3920	Sa	Sqw	0.3459	-0.1114	0.0720	0.2198	-0.0088	0.0215
3949	Sq	Sq	0.1761	-0.3090	0.1060	0.1596	0.0215	0.0086
4038		Vw	0.2529	1.1441	0.2926	-0.1791	0.1398	-0.0909
4055		V	0.0288	0.3319	1.1709	-0.2645	-0.1467	-0.0110
4142	A	L	0.1005	0.3651	-0.4177	0.0478	-0.3867	-0.0015
4179	Sk	Sq	0.1562	-0.1430	0.0974	0.0408	0.0416	-0.0098
4188	V	V	0.1660	0.4935	0.8254	-0.1066	0.1007	-0.0208
4197	Sq	Sq	0.0768	-0.0944	0.0891	-0.0621	-0.0056	0.0326
4352	S	S	0.1678	0.0187	0.0446	0.1405	-0.0021	-0.0004
4407	Sa	Sqw	0.3786	-0.1573	-0.0039	0.2266	-0.0549	0.0109
4417	S	Sw	0.2541	-0.0185	-0.0066	0.1849	-0.0371	0.0033
4451		Sv	0.2420	0.5906	-0.0221	-0.0264	0.0122	-0.0038
4558	S	Sr	0.1245	0.1072	0.0897	-0.0154	-0.0412	0.0029
4570	Sa	S	0.2440	0.2939	-0.1158	0.1608	-0.0636	0.0075
4688		Q	0.2132	-0.8539	0.3441	0.1742	-0.0777	0.0987
4713	A	Sw	0.4111	0.7832	-0.2321	0.0805	-0.0750	0.0388
4737	L	L	0.0665	0.7175	-0.3929	-0.0188	-0.0332	0.0214
4995	S	S	0.1258	0.1929	0.0414	-0.0337	-0.0116	-0.0002
5013	Sl	Sw	0.3330	0.0119	-0.0680	0.2286	0.0571	0.0177
5111	R	V	0.2066	0.5694	0.5980	-0.1307	-0.0110	0.0267
5143	O	O	0.0624	-0.7842	0.2619	0.1289	0.0385	0.0105
5230	S	S	0.1724	0.0673	0.0493	0.0494	-0.0373	0.0338
5261	Sr	Sa	0.4876	-0.9836	0.0731	0.2496	-0.1272	0.0817
5401	S	S	0.2466	0.3363	-0.0713	0.0723	0.0597	0.0195
5407	Sk	S	0.0610	0.1156	0.0172	-0.0276	0.0713	0.0066
5587	Sq	Sr	0.1093	-0.0387	0.1404	-0.0431	0.0934	-0.0007
5604		V	-0.0059	0.6429	0.8645	-0.1587	-0.0781	0.0369
5641	A	Sw	0.4133	0.2838	0.0066	0.1999	-0.0199	-0.0020
5660	Q	Q	0.1684	-0.7080	0.2413	0.2213	-0.1278	-0.0252
5685	S	S	0.1178	0.1648	-0.0382	0.0419	-0.0482	-0.0008
5817	S	Sr	0.1528	0.2990	0.0282	0.0697	-0.0362	0.0398
5840	Ld	L	0.0615	0.8321	-0.4394	0.0799	-0.1078	-0.0157
6047	S	S	0.1583	0.1579	0.0214	-0.0754	-0.1487	-0.0642
6239		Sqw	0.2828	-0.3266	0.1338	0.1199	0.0834	-0.0296
6386	S	S	0.2317	0.1362	-0.0010	0.1592	0.0515	-0.0416
6411		B	-0.1275	-0.2972	-0.1149	-0.1956	-0.0424	0.0111
6455	S	Srw	0.3291	0.4061	0.1819	0.2023	0.2276	-0.0038
6585	Sk	S	0.1147	0.0539	0.0586	0.0118	0.0238	0.0360
7341	Sq	Q	0.0773	-0.4510	0.1878	0.1417	-0.0197	-0.0155
7763	L	L	0.0369	0.5498	-0.3018	0.0234	-0.0294	-0.0188
8334	S	S	0.1609	0.0801	-0.0140	0.0857	0.0747	0.0277

Object	Bus Class	DeMeo Class	Slope	PC1'	PC2'	PC3'	PC4'	PC5'
8444		S	0.1777	0.2300	-0.0559	0.1410	-0.0224	0.0044
17274		X	0.4237	-0.3824	-0.0526	-0.2156	-0.0445	-0.0349
18736		Sw	0.2492	0.0387	0.0908	0.0723	0.1699	-0.0230
19127		Qw	0.2832	-0.3785	0.2522	-0.0087	-0.1720	-0.1393
19356	S	Sq	0.1229	-0.1385	0.1343	0.1090	-0.0537	0.0019
20786		Sq	0.0695	-0.3133	0.0392	-0.2523	-0.0629	-0.0224
20790		S	0.0486	0.2985	-0.0060	-0.0350	0.0465	-0.0096
22771		S	0.2264	0.6273	-0.1888	0.0128	0.0341	-0.0321
24475		Sw	0.2774	0.7547	-0.2018	0.1522	0.0178	-0.0313
35107		Sq	0.2409	-0.3046	0.1300	0.1665	0.0219	0.0273
36284		K	0.1107	-0.1968	-0.0413	0.0979	0.0223	-0.0324
53435		Srw	0.3577	0.3091	0.0856	-0.0179	0.0047	0.0077
54690		S	0.2020	0.5061	-0.2364	-0.0731	0.0468	0.0010
66146		Q	0.0858	-0.5855	0.1891	0.1026	-0.0367	-0.0099
86450		L	0.1180	0.3649	-0.2185	-0.0743	0.1205	-0.0517
86819		Sq	0.1680	-0.2950	0.1200	0.2179	-0.0268	-0.0452
89355		Sr	0.2111	0.2369	0.0799	0.0610	0.0568	0.0161
98943		Sw	0.3928	0.2022	-0.0203	0.0259	0.1419	-0.0436
137062	Sq	Sr	0.1011	0.3418	0.2032	0.2097	0.2369	0.0584
1989VA	Sq	Sr	0.1541	-0.1192	0.2803	0.1263	0.1758	0.0530
1997AE12		Q	0.1561	-0.5143	0.2280	0.1113	-0.0834	-0.0288
2000GD2		Q	0.0732	-0.3689	0.1455	0.0965	0.0418	-0.0597
2000PG3		D	0.4300	0.3343	-0.2655	-0.2128	0.0289	-0.0332
2000XL44		S	0.2240	-0.0382	0.0331	0.1544	0.0537	-0.0624
2001MQ3		K	0.1459	0.0640	-0.1642	0.0521	-0.2369	0.0169
2001TX16		X	0.2436	-0.0120	-0.1664	-0.2179	0.0668	-0.0506
2001XN254		S	0.1939	0.3016	-0.0733	0.0756	-0.0163	-0.0943
2002AA		S	0.0267	0.1247	0.0117	-0.0773	-0.0387	-0.0345
2002AV		S	0.1646	-0.0534	-0.0110	-0.0969	-0.0110	-0.0641